NATIONAL TECHNICAL UNIVERSITY OF ATHENS
SCHOOL OF NAVAL ARCHITECTURE & MARINE ENGINEERING

"NUMERICAL INVESTIGATION ON THE EFFECT OF BILGE KEELS IN SHIP ROLL DAMPING"

DIPLOMA THESIS

SPYROU IOANNIS-TARO

Supervisor: George Papadakis, Assistant Professor NTUA

ACKNOWLEDGMENTS

This thesis is the final requirement for the award of the diploma in Naval Architecture & Marine Engineering of the National Technical University of Athens.

This research would not be completed without the precious help of many other people. I would like to thank George Papadakis for introducing me to the principles of the Computational Fluid Dynamics and for his useful guidance and supervision. I would also like to thank Ph.D candidate Dimitris Ntouras for always being there for my questions, especially in these difficult times during the pandemic.

I would never be able to complete this research or even my studies without the economic and psychological support of my family, their love is truly appreciated. At last, I would especially like to thank my father for introducing me to the principles of ship stability and ship dynamics and my friend Antonis for sharing with me the same office throughout the course of this research, having priceless conversations and supporting mutually each other.

I.T. Spyrou, Athens 2020

This page intentionally left blank

CONTENTS

Nomenclature

2D : *Two dimensional*
3D : *Three dimensional*
DoF : Degrees of Freedom
CFD : *Computational Fluid Dynamics*
PIV : *Particle Image Velocimetry*
RANS : *Reynolds Averaged Navier-Stokes*
URANS : *Unsteady Reynolds Averaged Navier-Stokes*
VoF : *Volume of Fluid*
CFL : Courant Number
α_l **:** Phase volume fraction
$\ddot{\varphi}$ **:** Roll acceleration
$\dot{\varphi}$ **:** Roll velocity
μ : Dynamic viscosity
ρ : Density
ω : Angular frequency
φ : Roll angle
b : Damping coefficient
b_{eq} **:** Equivalent linearised damping coefficient
b_l **:** Linear damping coefficient
b_q **:** Quadratic damping coefficient
c : Restoring coefficient
I : Moment of Inertia
m : Mass
M_h **:** Hydrodynamic moment
M_{ext} **:** External moment
M_{tot} **:** Total moment
M_a **:** Moment due to added mass
M_b **:** Moment due to added damping
M_c **:** Restoring moment

p : Hydrodynamic pressure
u : Flow velocity
β : Artificial Compressibility factor

ABSTRACT

In engineering, there has always been a demand for accurate predictability of the dynamic responses of numerous dynamic systems. Being able to estimate the response of such systems is major in several aspects. More precisely, in Marine Engineering, in order to make a ship sufficiently safe for the crew and the cargo, you got to know how extreme the motion of the ship is going to be for the various ship designs that can be applied . To be able to predict the roll motion of a ship, which is the rotational oscillation around the longtitudinal axis, we need to know how and how fast the mechanical energy of the system is expelled. In ship stability, the quantity that represents the loss of energy of a rolling system is the *Roll Damping.*

To look deeper into *Roll Damping's* mechanisms, we need to understand the behavior of the fluid's motion around the ship's hull. This motion, for a viscous flow, is modeled by the *Navier-Stokes* equations. Our numerical solver , *MaPFLow,* is constructed to treat these equations numerically. It is an unstructured cell-centered finite volume solver, that solves the unsteady Reynolds Averaged Navier–Stokes (URANS) equations. *MaPFlow* considers the fluid *"artificially compressible"* in order to produce the coupling between pressure and velocity in the *Navier-Stokes* equations (Mass and Momentum Conservation). The simulations were performed allowing one degree of freedom to the barge (simulation's model). The free-surface is modeled using the Volume of Fluid (VoF) method and the second order differential equation which describes the motion of the rolling body is approximated by the 2^{nd} order Newmark-beta method.

Purpose of the present study is the determination of the roll damping coefficients of several 1-DoF free roll decay tests and the performance of multiple, wave excited, forced roll simulations using CFD. The motivations for this work were, to have a better understanding of how the bilge keels affect the natural period of a ship, the pressure and the vorticity field around it and how the generating vortices (caused by the rolling) are connected to the damping's mechanisms. For that reason, free roll decay tests with and without bilge keels were performed and their simulation's results were compared. In order to have an outlook of how the bilge keels affect the wave excited rolling system, regular waves were generated providing the hydrodynamic moment the barge needs to prepare forced roll tests also with and without bilge keels. In these tests no damping coefficients were extracted, although the dynamic responses were obtained and compared .

Περίληψη

Στη σύγχρονη μηχανική, υπήρχε πάντα η ανάγκη για έγκυρη προβλεψιμότητα των δυναμικών αποκρίσεων, για διάφορα δυναμικά συστήματα. Το να αποκτήσουμε τη δυνατότητα να εκτιμήσουμε τις αποκρίσεις τέτοιων συστημάτων είναι κρίσιμο για ποικίλους λόγους. Πιο συγκεκριμένα στη Ναυπηγική προκειμένου ένα πλοίο να είναι επαρκώς ασφαλές για το πλήρωμα και το φορτίο θα πρέπει κάποιος να γνωρίζει πόσο έντονες κινήσεις ενδέχεται να προκληθούν για τα διάφορα designs που μπορούν να εφαρμοστούν. Για το λόγο αυτό, γεννάται η ανάγκη να κατανοήσουμε πως και πόσο γρήγορα ένα πλοίο αποβάλλει ενέργεια καθώς εκτελεί διατοιχισμό, που είναι και το είδος της κίνησης που θα μας απασχολήσει. Το μέγεθος που αντιπροσωπεύει αυτή την απώλεια ενέργειας ονομάζεται απόσβεση διατοιχισμού.

Προκειμένου να εμβαθύνουμε στους μηχανισμούς που διέπουν την απόσβεση διατοιχισμού, θα πρέπει να κατανοήσουμε την κίνηση του ρευστού γύρω από την γάστρα ενός πλοίου. Αυτή η κίνηση, για ένα συνεκτικό ρευστό διέπεται από τις εξισώσεις Navier Stokes. Ο αριθμητικός επιλύτης μας, *MaPFlow*, είναι κατασκευασμένος για να προσεγγίζει αυτές τις εξισώσεις αριθμητικά. Βασίζεται στην αδόμητη κεντροκυψελική θεώρηση και επιλύει το μη ευσταθές RANS σύστημα εξισώσεων (URANS). Ο MaPFlow θεωρεί το ρευστό ψευδοσυμπιεστό προκειμένου να παράξει τη σύζευξη πίεσης και ταχύτητας η οποία δεν υφίσταται αν θεωρήσουμε το ρευστό ασυμπίεστο. Οι προσομοιώσεις έγιναν επιτρέποντας στο μοντέλο 1 βαθμό ελευθερίας. Η ελεύθερη επιφάνεια μοντελοποιήθηκε με τη μέθοδο Volume of Fluid (VoF) και η δευτεροτάξια εξίσωση της κίνησης διατοιχισμού προσεγγίστηκε από τη μέθοδο Newmark-beta.

Σκοπός της παρούσης εργασίας είναι ο καθορισμός των συντελεστών απόσβεσης διατοιχισμού για τις διάφορες προσομοιώσεις ελεύθερου διατοιχισμού και η εκτέλεση προσομοιώσεων εξαναγκασμένου, από αρμονικό κύμα, διατοιχισμού. Το κίνητρο ήταν κατά κύριο λόγο, το να αποκτηθεί μια πιο ευκρινής εικόνα του πως και κατά πόσο επιδρούν τα παρατροπίδια (bilge keels) στους μηχανισμούς της απόσβεσης διατοιχισμού καθώς και στη φυσική ιδιοπερίοδο ενός πλοιο. Για το λόγο αυτό προσομοιώσεις ελεύθερου διατοιχισμού εκτελέστηκαν και οι συντελεστές απόσβεσής τους συγκρίθηκαν, ενώ στις περιπτώσεις του εξαναγκασμένου διατοιχισμού συγκρίθηκαν οι αποκρίσεις.

This page intentionally left blank

1.INTRODUCTION

1.1.THE IMPORTANCE OF HAVING AN ACCURATE ROLL DAMPING PREDICTION

Roll damping is a complex process of energy transfer which affects the amplitude of motion of a ship. To determine the damping during a roll motion we have to take in consideration viscous effects, caused by the interaction of the fluid and the rolling body but also effects caused by the interaction of the body and the free surface. To mitigate roll motion it is customary to install on a ship's hull bilge-keels.

Bilge keels are thin objects made of steel and placed at the bilge of a ship in order to increase the damping of the ship's roll motion. Naval architects have used bilge keels for many years as a tool to decrease large roll amplitudes in ships because large roll angles are unsafe, especially for container ships and cruise ships. Roll damping is also a major factor contributing in resonance phenomena of rotating bodies, giving us useful information for the calculation of the safe oscillating frequency area of the body. If resonance or extreme roll motion occurs it may cause cargo loss, ship damage, crew injuries or even capsize. All the above make the demand for a roll damping prediction method necessary for naval architecture.

Historically, several incidents involving excessive rolling have been recorded:

In February 13, 2014 M/V Svendborg Maersk a Danish-flagged 8,160 TEU container ship departed from Rotterdam's port bound for the Suez canal and the Far East. After exiting the English Channel the next day (February 14) she encountered adverse weather conditions heavier than the forecast had predicted causing a roll amplitude up to 40 angles in about 6-8 periods, which is extremely quick. Although the ship was equipped with bilge keels, the damping which they generated was proven insufficient. About 517 TEU were lost, another 250 were found severely damaged and the ship was assessed as unsafe by the master and proceeded to Malaga, Spain where it arrived on February 17.

To be able to predict or prevent large roll angles and roll accelerations, it is crucial to understand the physical principles of roll motion and especially roll damping. Our approach to compute the viscous roll damping is based on the Computational Fluid Dynamics (CFD) numerical methods which provide high precision results. However, such methods incur a much higher computational cost than the traditional modeling methods. As a result CFD modeling is not yet widely used at the design stage of a ship.

1.2.PURPOSE OF THE STUDY

The obvious objective of this thesis, is to develop a reliable CFD model, able to calculate roll damping in various situations, within an acceptable simulation time. Although the phenomena taking place around a rolling body are 3D, and comparing to our 2D approach there is a loss of information in these simulations, strip theory can be applied, by modeling multiple sections of the ship, to determine the actual loss of energy in the 3D problem.

Looking deeper at the roll damping,by being able to visualize and observe the rolling of a ship or a ship model, using CFD tools, we can have a deeper understanding of the physical principles concerning roll damping and its relation with the vorticity developing around the hull. Moreover, we can observe how the bilge keels affect the vorticity field and the damping in total. Having a deeper understanding of these mechanisms can guide us to optimize the hull's and the bilge keel's design, concerning roll damping, in the future.

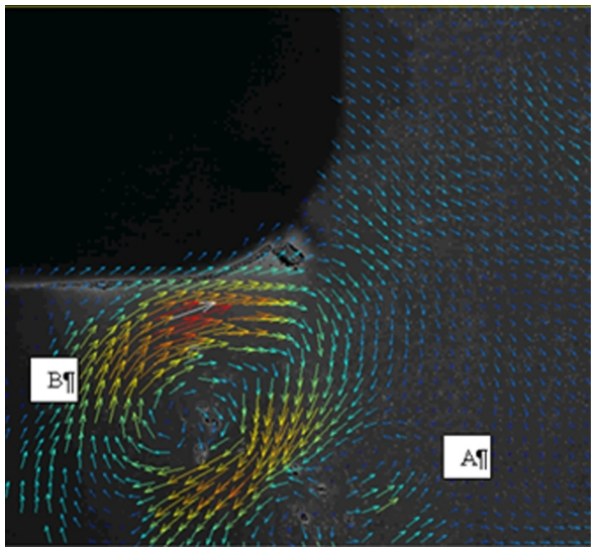

Figure 1.1: Typical PIV of the velocity field around bilge keel during roll motion

The following paragraph provides a short overview of the subjects this thesis is going to analyze and a brief summary of what the following chapters contain:

- **Literature Review :** A short presentation of prior work done on roll damping by various researchers along with the physical principles of roll damping are provided in Chapter 2.

- **Numerical Method :** In Chapter 3, the theory behind the CFD algorithm *"MaPFlow"*, will be discussed.

- **Computations :** All the calculations concerning the damping, the roll simulations performed by *MaPFlow* along with our conclusions and proposals for future work on the field are contained in Chapter 4.

2.LITERATURE REVIEW

2.1.BACKGROUND

To make a ship both safe and habitable, roll response needs to be accurately estimated. As we may have already mentioned roll damping is a major factor contributing in the motion of a rolling body. It seems that the first attempt to take roll damping in consideration , in the approach to predict the roll response of a ship, was by William Froude. Froude's observations on roll motion, led to the proposal of bilge keels in the late 1800s.

The literature on roll damping is largely empirical. Although many researchers have investigated the topic of ship roll damping since Froude's attempts, it was the Japanese back in the 1950's and even before that investigated the various aspects of ship roll damping in a systematic and detailed manner. In the late 1970's *Ikeda*, *Himeno* and *Tanaka* all from *Osaka Prefecture University* in Japan published several papers [1], [2], all of them summarizing the work done by others, presenting a fundamentally new practical estimation technique for roll damping, namely the *Ikeda method (1978)*. This method separates the damping components neglecting their interactions. The roll damping components according to *Ikeda* were the wave, the eddy making, the frictional, the bilge keel's and the linear lift (for a ship at forward speed).

A few years later, in 1981, Prof. Himeno produced his comprehensive report [3] on ship roll damping (Himeno 1981). This report included a very complete literature survey of both Japanese and non-Japanese literature on the topic and two computer programs to predict ship roll damping. The first computer program is a simple method based only upon ship and bilge keel characteristics. However, the second computer program is more complete and involves the component-wise approach. As a result of the systematic and comprehensive approach of the Japanese this methodology is by far the most popular. Ikeda has continued work on roll damping prediction until this day (Kawahara et al. 2012). Unfortunately the Himeno report and associated computer programs are

well-known to have numerous typographical errors and it is suggested to verify all equations with the original references. Another shortcoming of the method noted is that the methods are for general cargo ship hulls and may not be applicable to shallow draft high beam to draft ratio transport barges and other similar vessels.

In response to the wide use of transport barges(***Fig.1.2***) in the offshore industry in the mid-1980's several investigations centered on a Noble Denton Joint Industry Project were undertaken. The focus of this effort was both model testing and predicting eddy damping of barges with sharp corner bilges using a vortex method. The development of this vortex method was done jointly by Standing, (1991) at British Marine Technology (BMT) and several faculty and graduate students at Imperial College London (Downie et al. 2006). Several papers described the method in various stages of development and also include comparisons to the Japanese empirical prediction methods of Ikeda et al. (1978) and Tanaka and Hishida (1960, 1959, 1957a, 1957b). The so-called Noble-Denton method of predicting roll damping is one of many vortex shedding based methods (Standing 1991). These methods are only strictly applied to sharp bilge corner transport barges. However, in an effort to make these methods more broadly applicable an empirical correction has been developed to account for a finite bilge radius (Robinson and Stoddart 1987). Unfortunately, the relatively good results achievable with these methods for square bilges are not generally achievable for barges of finite bilge radius.

Figure 1.2: Typical Transport Barge

2.2.MORE RECENT STUDIES

The estimation of roll damping from empirical relations based on model tests gained popularity in the 1970's and 1980's. A simple theoretical method based on experimental results, also known as Ikeda's method, was developed and is recommended by the ITTC International Towing Tank Conference (2011). It has become the most popular method to predict the energy dissipation using potential theory. Nevertheless, the empirical coefficients provided by the method are based on former typical hull geometries. Furthermore the formula is not applicable in ships with high position of their center of gravity or long natural roll period and a modified method is proposed to improve accuracy.

Although these methods are widely used, the theoretical assumptions that have to be made, the simplicity of the hull forms for which we can apply them and the lack of consideration of other ship parameters set their value to be limited. In order to improve the precision of the predictions numerous approaches of CFD modeling have been attempted to calculate roll damping.

CFD has been used to calculate roll damping as early as 1997 by Falzarano et al. [4]. However, only in recent years, extensive research has been done in this field. The use of numerical methods in the calculation of the viscous flow around ships and other floating bodies did not start long ago. Vortex tracking method was used to study the effect of viscosity and separated flows around rectangular body with sharp corners [5] (Braathen and Faltinsen, 1988). About 20-25 years later, two dimensional (2D) incompressible Navier-Stokes solver had been used to simulate the viscous flow around a rolling hull (Avalos et al., 2014; Bangun et al., 2010; Irkal et al., 2014; Kinnas et al., 2006; Yu and Kinnas, 2009).

Moreover, Jaouen et al. [6] predicted the roll added mass and damping coefficient using a 2D unsteady Reynolds averaged Navier-Stokes (URANS) CFD code named ReFRESCO without taking wave-making damping into account. This wave-making damping is subtracted using potential flow theory by assuming the separate damping components can be linearised as stated by Ikeda et al. [1]. The results show good agreement with the test data of Ikeda et al. [1].

Jaouen et al. [7] continued their research and found that the viscous damping coefficient varies linearly with the roll response amplitude for low dimensionless frequencies. Just as in their previous research, the wave-making effect is not taken into account. They achieved this by mirroring the hull section at the water plane. Jaouen et al. [7] also researched the viscous scale effect. The difference between the viscous damping coefficient between the model scale and full scale turns out to be 1.85%. One side note regarding this is that for the model scale tests, no wall models were used, where, in the full-scale tests, wall models were used which decrease the accuracy of the model.

2.3.PHYSICS OF THE ROLL MOTION AND DAMPING

2.3.1.Roll Motion

As Belibasakis and Athanasoulis describe [8], in ship dynamics when a ship or any rigid body is free-floating we say that it moves in six degrees of freedom. That means, its motion will be decided by the solution of the 6x6 coupled system of differential equations for the respective degrees of freedom. More precisely, there are three transportational types of motion namely:

• **Surge**, motion in the forward and backward direction, x-axis, positive forward
• **Sway**, motion in the sideways directions, y-axis, positive to port side
• **Heave**, motion in upward and downward direction, z-axis, positive upward

Furthermore, there are three rotations which are defined as:

• **Roll**, rotation around the x-axis, positive right turning
• **Pitch**, rotation around the y-axis, positive right turning
• **Yaw**, rotation around the z-axis, positive right turning
In **Figure 2.1** an overview of the 6 degrees of freedom of a ship is provided .

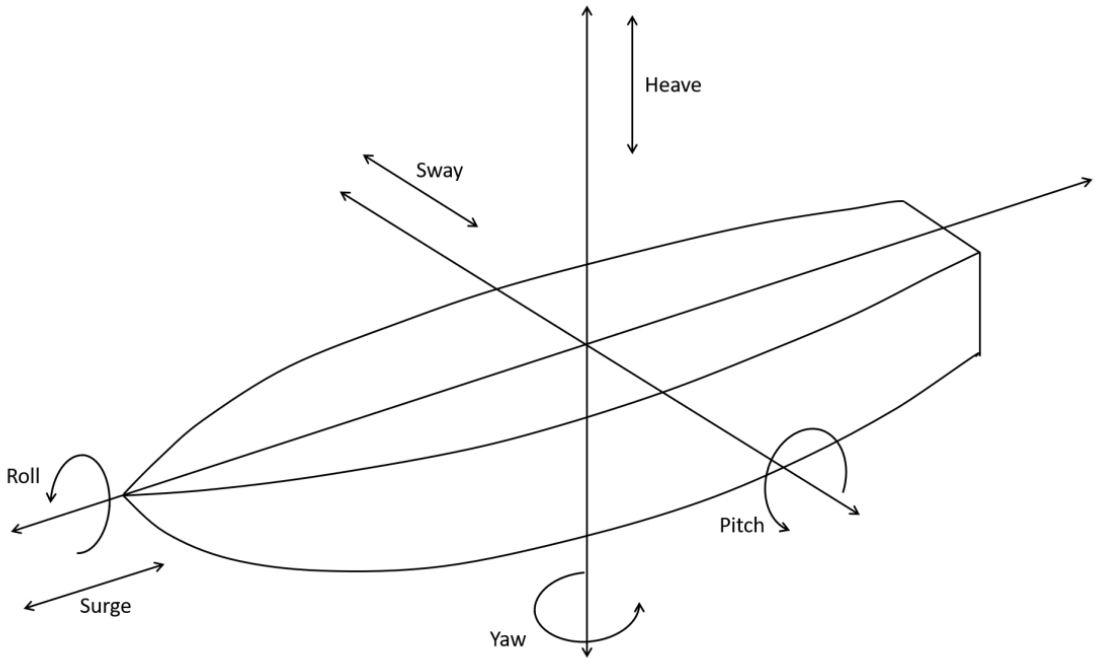

Figure 2.1:The six-degree of freedom ship motion

Although **Figure 2.1** prepares us for roll motion to be fixed about the *x*-axis, the real roll axis is parallel to the *x* and passes through the center of flotation(LCF), which is the centroid of the area of the water plane. The interaction between the ship and the fluid, during rolling, generates two types of forces, the pressure force, $\boldsymbol{F_p}$, in normal direction and the viscous or friction force, $\boldsymbol{F_f}$, in tangential direction as visualised in **Figure 2.2**. The integration of these forces over the structure surface generates a buoyancy force $\boldsymbol{F_b}$ and a restoring moment $\boldsymbol{M_\varphi}$ around a longitudinal-axis through the centre of rotation, which is defined by the centre of buoyancy and the centre of gravity. The centre of buoyancy and the centre of gravity are presented as the black dot at the beginning of the $\boldsymbol{F_b}$ vector and the black dot at the beginning of the $\boldsymbol{F_g}$ vector respectively.

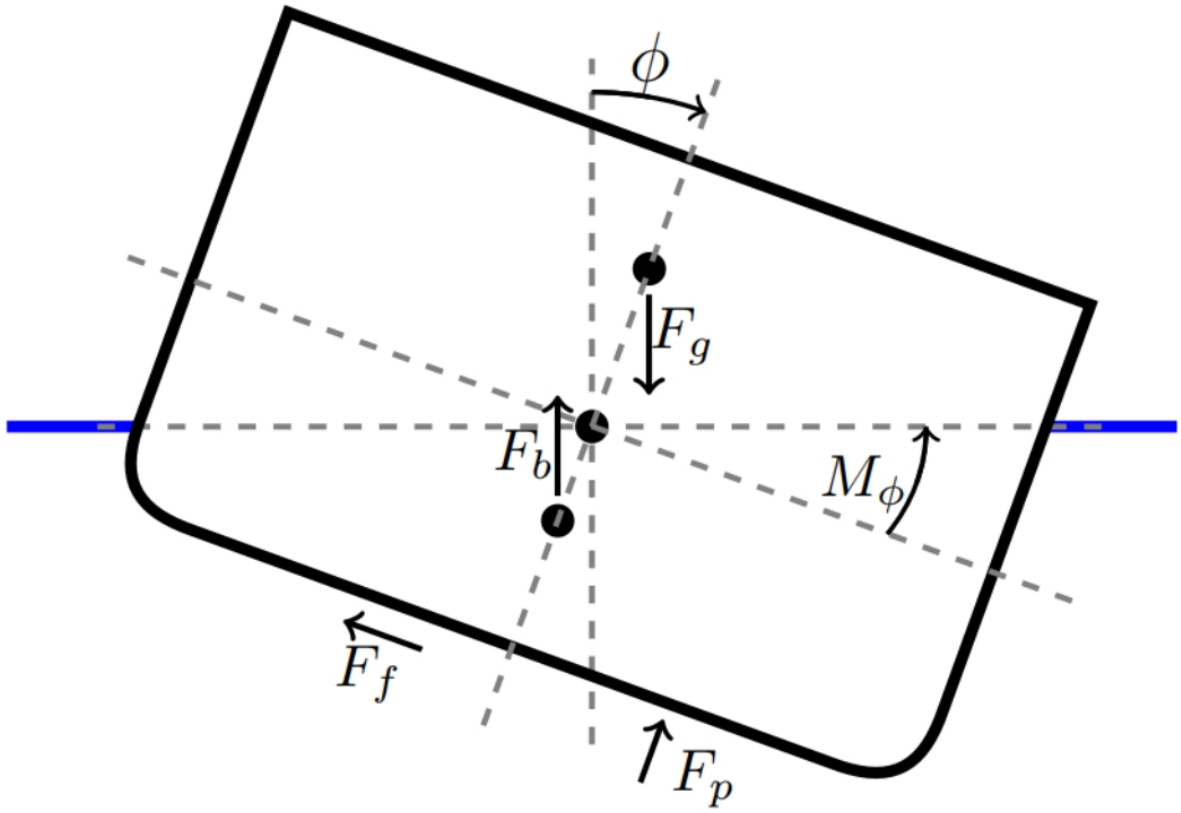

Figure 2.2: Forces acting during rolling

The type of problem *MaPFlow* solves, using the Newmark-beta method of numerical integration, as Manolas et. al [9] suggests, is presented below (eq. (2.1)),

(2.1) $$M_{tot} = I\ddot{\phi}$$

Where I is the inertia and $\ddot{\varphi}$ is the roll acceleration. By splitting $\boldsymbol{M_{tot}}$ in an external moment $\boldsymbol{M_{ext}}$ and a moment due to the forces of the water $\boldsymbol{M_h}$, Equation (2.2) is obtained.

(2.2) $$M_{ext} - M_h = I\ddot{\phi}$$

The term $\boldsymbol{M_h}$ represents the moment occurring by all the hydrodynamic forces caused by the fluid both due to potential and viscous flow, and is expressed as:

(2.3) $$M_h = \int_S \mathbf{r} \times \left(-pI + \bar{\bar{\tau}} \right) \hat{\mathbf{n}} dS$$

Because $\boldsymbol{M_h}$ in Equation (2.2) refers to all the forces acted on the structure by the water $\boldsymbol{M_h}$ can also be expressed as:

(2.4) $$M_h = M_a(\ddot{\phi}) + M_b(\dot{\phi}) + M_c(\phi)$$

Where M_a is the moment produced by the added mass of the oscillator, M_b the moment due to the damping of the system and M_c the restoring moment of the ship. The calculation of M_h is important for the determination of the damping coefficients of a wave excited forced roll oscillator.

The roll motion of a ship around its longitudinal axis can be regarded as a dynamical system. The energy and motion state of this system is defined by roll angle φ, roll angle velocity $\dot{\varphi}$ and angular acceleration $\ddot{\varphi}$. The properties of the roll motion behavior are determined by the hull shape, the mass distribution and the motion of the surrounding water. The effect of the system that causes the decrease of the roll angle amplitude, is termed roll damping and is caused by many flow effects: wave radiation, viscous friction, eddy separation, lift effects (if the ship operates at forward speed) , bilge keels etc. To be able to predict or prevent large roll angles and roll acceleration, it is important to understand the physical principals of roll motion and especially roll damping.

2.3.2.Roll Damping

For the last fifty years the research on the physical principles of roll damping has grown. In 1978 *Ikeda, Himeno and Tanaka* on their study "Components of Roll Damping of Ship at Forward Speed" proposed four damping components mainly due to the fluid viscosity, namely the frictional (B_F) , the wave (B_W), the bilge keel (B_{BK}), the eddy making (B_E), at zero forward speed, and at forward speed the linear lift component is added (B_L). The damping components were derived from simplified formulae obtained form related theory and model experiments.

(2.5) $$b = b_f + b_e + b_L + b_w + b_{bk}$$

In physical terms the roll damping represents the loss of rotational energy of a ship. The amount of this energy loss is specified by the damping coefficient (or coefficients) of the system. However, an even more precise parameter giving us a much more clear estimation of the system's damping is the damping ratio ζ. The damping ratio ζ stands for the non-dimensional damping of the oscillator. More precisely, the 0 value of ζ means there is no damping force acting in the oscillation and ζ=1 value means the motion of the body isn't oscillatory. The damping ratio is a parameter observed in a linear roll model. In a free roll decay test the linear differential equation describing the motion of a 1 DoF ship is shown in eq. (2.6) along with the damping ratio ζ of the system.

$$\frac{d^2\varphi}{dt^2} + 2\zeta\omega_n \frac{d\varphi}{dt} + \omega_n^2\varphi = 0. \qquad (2.6)$$

The above linear expression can describe pretty accurately the roll motion of a one degree of freedom body oscillating in water in low roll amplitudes. Although, as the initial angle increases the linear approximation we made becomes weaker. Furthermore, adding a bilge keel at a body's bilge radius increases even more the non linear effects on the system. For these reasons, a non linear damping analysis had to be implemented in this work, in order to calculate damping efficiently. A useful tool for the determination of the system's damping, in such cases, is the *equivalent linear damping coefficient.* In our study we will assume that the damping moment has a 2nd order relation with the roll angle as shown in equation (2.7).

$$(I + A)\ddot{\phi} + B_1\dot{\phi} + B_2\dot{\phi}|\dot{\phi}| + C\phi = 0 \qquad (2.7)$$

The higher order terms of the damping are not expected to be significant in comparison to the linear term and that is the reason the 2nd order approximation was used. The quadratic damping coefficient will be calculated from the decay curve by comparing the energy loss in an oscillating cycle to the work done by the damping force, concerning the free decay roll tests.

3.NUMERICAL METHOD

3.1. NUMERICAL SOLVER : MaPFlow

MaPFlow is an Eulerian numerical solver made in NTUA(National Technical University of Athens) to encounter multiphase flow and FSI(Fluid-Structure Interaction) problems, based on the Eulerian fluid mechanics approach. *MaPFlow* can be used to calculate both inviscid and viscous flows around submerged or floating bodies for a compressible or an incompressible fluid in a 2-D or a 3-D situation. In case we consider the fluid to be incompressible, the Navier-Stokes Energy equation is degenerated. The coupling between the velocity and the pressure in the Mass and the Momentum equations is now lost and we need a new tool to produce it in order to be consistent with the physical problem. For that reason the Artificial Compressibility method has been developed and will be implemented in our study to come up against this inconsistency.

In order to calculate the dynamic response in a FSI problem it's necessary to approach the 2nd order differential equation of the oscillator in a numerical manner. The reason for this is that the total force or the total momentum, in the rotating oscillator case, is calculated using numerical integration methods for both the convective and the viscous parts.

3.1.1.Governing equations

3.1.1.1 Artificial Compressibility

As Ntouras and Papadakis suggest [10], to deal with the pressure and velocity being uncoupled in the incompressible problem we will use the artificial compressibility factor β and so,

For one phase viscous flows the governing equations take the form:

Continuity:

$$\frac{1}{\rho\beta}\frac{\partial p}{\partial \tau} + \nabla \cdot \vec{v} = 0 \tag{3.1}$$

Momentum:

$$\frac{\partial \vec{v}}{\partial t} + \vec{v} \cdot \nabla \vec{v} = -\frac{\nabla p}{\rho} + \nabla \bar{\sigma} + \vec{F}_B \tag{3.2}$$

Additionally, for two phase flows in order to model the free surface, the Volume of Fluid method has to be implemented and so one more transport equation needs to be solved.

$$\frac{\partial \alpha_l}{\partial t} + \vec{v} \cdot \nabla \alpha_l = 0 \tag{3.3}$$

As a fluid in a control volume can only have one density and one viscosity value an interpolation is made as given in (4)

$$\begin{aligned} \rho_m &= \alpha_l \rho_w + (1 - \alpha_l)\rho_a \\ \mu_m &= \mu_l \rho_w + (1 - \alpha_l)\mu_a \end{aligned} \tag{3.4}$$

Where,

$$\alpha_l = \frac{\rho - \rho_a}{\rho_w - \rho_a}$$

3.1.1.2.Derivation of Conservative form

Considering the compressible form of the mass continuity equation, adding the fictitious time derivative:

(3.5)
$$\frac{\partial \rho}{\partial t} + \frac{\partial \rho}{\partial \tau} + \nabla \cdot (\rho \vec{v}) = 0$$

The above expression is only valid though, when $\frac{\partial \rho}{\partial \tau} = 0$
Expanding the terms of the mass equation,

(3.6)
$$\cancel{\frac{\partial \rho}{\partial t}}^{0} + \frac{\partial \rho}{\partial \tau} + \rho \nabla \cdot \vec{v} + \vec{v} \cdot \cancel{\nabla \rho}^{0} = 0 \rightarrow$$
$$\frac{\partial \rho}{\partial \tau} + \rho \nabla \cdot \vec{v} = 0$$

Using the artificial compressibility constitutional equation,

(3.7)
$$\frac{\partial \rho}{\partial p} = \frac{1}{\beta}$$

the equation (6) becomes now

(3.8)
$$\frac{1}{\rho\beta}\frac{\partial p}{\partial \tau} + \nabla \cdot \vec{v} = 0$$

The conservative form of the Navier-Stokes momentum equation, adding the fictitious time derivative is shown below,

(3.9)
$$\frac{\partial (\rho\vec{v})}{\partial t} + \frac{\partial (\rho\vec{v})}{\partial \tau} + \nabla (\rho\vec{v} \cdot \vec{v}) = -\nabla p + \nabla\bar{\sigma} + \vec{F}_B$$

And as we analyze the temporal term,

(3.10)
$$\begin{gathered}\frac{\partial (\rho\vec{v})}{\partial t} = \rho\frac{\partial \vec{v}}{\partial t} + \vec{v}\frac{\partial \rho}{\partial t} \longrightarrow \\ \frac{\partial (\rho\vec{v})}{\partial t} = \rho\frac{\partial \vec{v}}{\partial t} + \vec{v}\frac{\partial}{\partial t}(a_l\Delta\rho + \rho_a) \rightarrow \\ \frac{\partial (\rho\vec{v})}{\partial t} = \rho\frac{\partial \vec{v}}{\partial t} + \vec{v}\Delta\rho\frac{\partial a_l}{\partial t}\end{gathered}$$

Similarly the pseudo-time derivative becomes:

(3.11)
$$\frac{\partial\left(\rho\vec{v}\right)}{\partial\tau}=\rho\frac{\partial\vec{v}}{\partial\tau}+\vec{v}\Delta\rho\frac{\partial a_l}{\partial\tau}$$

Finally, the transport equation for the volume fraction using eq. (3.1)

(3.12)
$$\frac{\partial\alpha_l}{\partial t}+\frac{\partial\alpha}{\partial\tau}+\frac{\alpha_l}{\rho_m\beta}\frac{\partial p}{\partial\tau}+\nabla\left(\vec{v}\alpha_l\right)=0$$

By integrating in a reference volume Ω the equations (3.8), (3.10), (3.11), (3.12) the system of equations can be now written as,

$$\Gamma\int_\Omega\frac{\partial\overrightarrow{Q}}{\partial\tau}\mathrm{d}\Omega+\Gamma_e\int_\Omega\frac{\partial\overrightarrow{Q}}{\partial t}\mathrm{d}\Omega+\int_{\partial\Omega}\left(\overrightarrow{F}_c-\overrightarrow{F}_v\right)\mathrm{d}S=\int_\Omega\overrightarrow{S}_q\mathrm{d}\Omega$$

(3.13)

where the matrix Γ is the preconditioning matrix, which is also used to compute the convective fluxes in order to remove the density dependency from the eigenvalues of the system. The matrix Γ_e is the Jacobian matrix $\Gamma_e=\frac{\partial\overrightarrow{U}}{\partial\overrightarrow{Q}}$.

(3.14)
$$\Gamma=\begin{bmatrix}\frac{1}{\rho_m}&0&0\\0&\rho_m I&\vec{v}\Delta\rho\\\frac{\alpha_l}{\rho_m}&0&\beta\end{bmatrix}\quad,\quad\Gamma_e=\begin{bmatrix}0&0&0\\0&\rho_m I&\vec{v}\Delta\rho\\0&0&\beta\end{bmatrix}$$

The unsteady system of equations is expressed for the conservative variables [..] , in each pseudo steady time-step a system of equations for the primitive variables [..] is solved.

$$\overrightarrow{U} = \begin{bmatrix} 0 & \rho\vec{v} & \alpha_l \end{bmatrix}^T \qquad \overrightarrow{Q} = \begin{bmatrix} p & \vec{v} & \alpha_l \end{bmatrix}^T$$

$$\frac{\partial \overrightarrow{U}}{\partial t} = \Gamma_e \frac{\partial \overrightarrow{Q}}{\partial t}$$

(3.15)

The inviscid and viscous fluxes are described as shown below,

$$\overrightarrow{F_c} = \begin{bmatrix} V_n \\ \rho_m u V_n + p n_x \\ \rho_m v V_n + p n_y \\ \rho_m w V_n + p n_z \\ \alpha_l V_n \end{bmatrix} \qquad \overrightarrow{F_v} = \begin{bmatrix} 0 \\ \tau_{xx} n_x + \tau_{xy} n_y + \tau_{xz} n_z \\ \tau_{yx} n_x + \tau_{yy} n_y + \tau_{yz} n_z \\ \tau_{zx} n_x + \tau_{zy} n_y + \tau_{zz} n_z \\ 0 \end{bmatrix}$$

(3.16)

and the viscous stresses τ_{ij} ,

(3.17)
$$\tau_{ij} = (\mu_m + \mu_t)\left(\frac{\partial u_i}{\partial x_j} + \frac{\partial u_j}{\partial x_i}\right) - \frac{3}{2}\rho\delta_{ij}k$$

where μ_t is the turbulent dynamic viscosity, k is the turbulent kinetic energy and δ_{ij} is the Kronecker delta.

3.1.2. Discretization

3.1.2.1 Finite Volume Method

As mentioned, in order to calculate the flow variables (p,u,v,a_l) we have to approach equation (13) in a numerical way. For that reason the *Finite Volume Method (FVM)* will be implemented in our study. To apply the *FVM*, there is a demand for a cell-centered formulation on an implicit scheme. So, for a control volume Ω_I the finite volume method implies:

$$\overrightarrow{\overline{Q}} = \frac{1}{\Omega_I} \int_{\Omega} \overrightarrow{Q}\left(\vec{x}; t\right) \mathrm{d}\Omega \tag{3.18}$$

If u_{vol} is the velocity of the control volume, then from the Reynold's Transport Theorem

$$\begin{aligned} \frac{\partial}{\partial t} \int_{\Omega_I(t)} \overrightarrow{Q} \mathrm{d}\Omega = \int_{\Omega_I(t)} \frac{\partial \overrightarrow{Q}}{\partial t} \mathrm{d}\Omega + \int_{\Omega_I(t)} \nabla \left(\overrightarrow{Q} \cdot \vec{u}_{vol} \right) \mathrm{d}\Omega = \\ \int_{\Omega_I(t)} \frac{\partial \overrightarrow{Q}}{\partial t} \mathrm{d}\Omega + \oint_{\partial \Omega_I(t)} \overrightarrow{Q} \left(\vec{u}_{vol} \cdot \vec{n} \right) \mathrm{d}S \end{aligned} \tag{3.19}$$

Assuming that the Jacobian matrix Γ_e is constant inside the control volume, then by setting the grid velocity as $V_g = \vec{u}_{vol}\,\vec{n}$ and using the Reynold's transport theorem the temporal term becomes

$$\Gamma_e \int_{\Omega_I(t)} \frac{\partial \vec{Q}}{\partial t} \mathrm{d}\Omega = \int_{\Omega_I(t)} \frac{\partial \vec{U}}{\partial t} \mathrm{d}\Omega = \frac{\partial}{\partial t} \int_{\Omega_I(t)} \vec{U} \mathrm{d}\Omega - \oint_{\partial\Omega_I(t)} \left(\vec{U} V_g\right) \mathrm{d}S \qquad (3.20)$$

Substituting back to the original equation,

$$\Gamma_e \frac{\partial}{\partial t} \int_{\Omega_I(t)} \vec{Q} \mathrm{d}\Omega + \Gamma \frac{\partial}{\partial \tau} \int_{\Omega_I(t)} \vec{Q} \mathrm{d}\Omega = -\vec{R}_\Omega \qquad (3.21)$$

Where R_Ω is called residual of the equations expressed on the control volume Ω and takes the form,

$$\vec{R}_\Omega = \int_{\partial\Omega_I(t)} \left(\vec{F}_c - V_g \vec{U} - \vec{F}_v\right) \mathrm{d}S - \int_{\Omega(t)} \vec{S}_q \mathrm{d}\Omega \qquad (3.22)$$

Using the finite volume formulation (18) , equation (21) is now written as,

$$\Gamma_e \frac{\partial \left(\vec{\bar{Q}}\Omega\right)}{\partial t} + \Gamma \frac{\partial \left(\vec{\bar{Q}}\Omega\right)}{\partial \tau} = -\vec{R}_\Omega \qquad (3.23)$$

3.1.2.2. Spatial discretization

In every spatial mesh, which consists of arbitrary shape cells, a control volume $\boldsymbol{\Omega_I}$ can be defined for every grid element. So the boundaries of the control volume are the edges of the elements and the center of the control volume is the center of the element. The surface integral of the residual $\boldsymbol{R_\Omega}$ can be assumed constant in each edge and so the calculation of the integral is up to the calculation of the sum of the fluxes evaluated at the midpoint of the flux. Moreover, the volume integral (in the general 3-D case) of the control volume, which mainly consists of source terms and body forces , is also considered to be constant in each finite volume. So for a control volume consisting of $\boldsymbol{N_f}$ number of edges the right hand side of the equation (23) takes the form,

(3.24)
$$\vec{R}_{\Omega_I} \simeq \sum_{j}^{N_f} \left(\vec{F}_c - \vec{U}V_g - \vec{F}_v\right)_j \Delta S_j - \Omega_I \vec{S}_q$$

or by re-evaluating the inviscid fluxes to take in acount, also, the moving grid term

$$\vec{F}_c = \begin{bmatrix} V_n \\ \rho_m u\left(V_n - V_g\right) + pn_x \\ \rho_m v\left(V_n - V_g\right) + pn_y \\ \rho_m w\left(V_n - V_g\right) + pn_z \\ \alpha_l\left(V_n - V_g\right) \end{bmatrix}$$

the integral can now be written as,

(3.25) $$\vec{R}_{\Omega_I} \simeq \sum_{j}^{N_f} \left(\vec{F}_c - \vec{F}_v\right)_j \Delta S_j - \Omega_I \vec{S}_q$$

3.1.2.3.Convective Fluxes

For the calculation of the convective fluxes *MaPFLow* uses the approximate Rieman solver of Roe, combined with the preconditioned matrix **Γ**. Let $\boldsymbol{A_c}$ be the convective Jacobian matrix,

(3.26) $$\mathrm{A}_c = \frac{\partial \vec{F}_c}{\partial \vec{Q}} = \Gamma\Gamma^{-1} A_c = \Gamma \tilde{A}_c$$

then the flux across an edge *j* is computed as,

(3.27) $$\vec{F}_{c,j} = \frac{1}{2}\left(\vec{F}_c\left(\vec{Q}_R\right) + \vec{F}_c\left(\vec{Q}_L\right)\right) - \frac{1}{2}\overline{\Gamma\left|\tilde{A}_c\right|}\left(\vec{Q}_R - \vec{Q}_L\right)$$

where $|\boldsymbol{A_c}|$ is the Roe averaged-precoditioned jacobian:

(3.28) $$\left|\tilde{A}\right| = \tilde{R}^{-1}\left|\tilde{\Lambda}\right|\tilde{R}$$

where $\boldsymbol{R}$, $\boldsymbol{R^{-1}}$, $\boldsymbol{\Lambda}$ are the right, left eigenvectors and the eigenvalues of the preconditioned matrix . The eigensystem is evaluated by taking the average of the two neighbours that share the edge *j*

(3.29)
$$\tilde{Q}_j = \frac{Q_{j,R} + Q_{j,L}}{2}, \quad j = 1, 2, 3, 4, 5$$

3.1.2.4.Reconstruction of Variables

In order to compute the fluxes appearing at the right hand side of expression (3.25) the values of all the flow variables at the face centers have to be known. However, we miss this information, since all flow variables are defined at the cell centers of each control volume. Passing the flow information from the cell centers to the faces is carried out by a reconstruction scheme that extrapolates the cell centered values of the volume in the respective edge.

Consider a control volume $\boldsymbol{\Omega_i}$ and its neighbour $\boldsymbol{\Omega_j}$, with the normal of the face pointing from $\boldsymbol{\Omega_i}$ to $\boldsymbol{\Omega_j}$. We need to find the vectors $\boldsymbol{Q_L}$, $\boldsymbol{Q_R}$ with an extrapolation scheme based on the cells i,j respectively.

Piecewise Linear Reconstruction (PLR)

The velocity field is approximated through a piecewise linear interpolation scheme, given by equation (3.30). Since the surface tension is neglected, the velocity field is continuous even across the free surface. For this reason, the gradients are retained, and no limiter is applied.

(3.30)
$$\vec{Q}_L = \vec{Q}_i - \nabla\vec{Q}_i \cdot \vec{r}_i$$
$$\vec{Q}_R = \vec{Q}_j + \nabla\vec{Q}_j \cdot \vec{r}_j$$

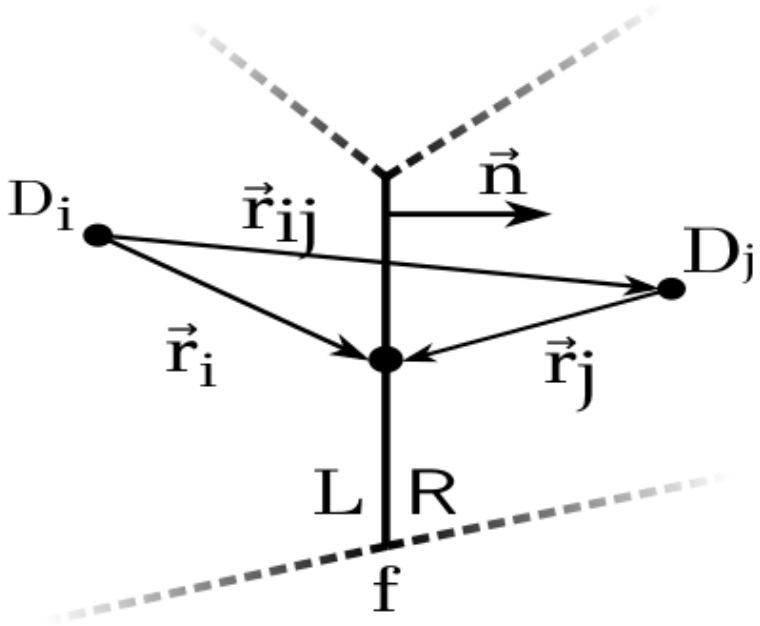

Figure 3.1: Reconstruction of Variables in face f

The vectors $\boldsymbol{r_i}$, $\boldsymbol{r_j}$ are pointing from the center of the control volume to the midpoint of the respective edge, as shown in ***Fig.3.1*** **.** For the calculation of the gradient of the flow variables, the least square method was implemented. The Green-Gauss theorem could also be appropriate to use for the calculation.

Furthermore, the pressure field is a continuous function in space, since surface tension is neglected. However, the pressure gradient is discontinuous across the free surface, due to the density jump. The condition with which we must comply is $[\nabla \boldsymbol{p}/\boldsymbol{\rho}]=0$. Researchers, have proposed several different schemes to come up against this difficulty by adopting a density-based interpolation scheme. In MaPFlow, the work of Queutey et al. [11] is followed. This scheme is introduced only near the free surface, while in the rest of the computational domain a piecewise linear interpolation scheme is used, similar to Equation (3.33).

Finally, of great importance is the reconstruction of volume fraction field ($\boldsymbol{\alpha_l}$). In order to reduce the numerical diffusion, it is important to adopt a compressive reconstruction scheme. Over recent decades, numerous reconstruction schemes have been introduced which offer low numerical diffusion. The requirements they should meet is boundedness and high accuracy even in large **CFL** numbers. Most of these reconstruction schemes are based on Leonard's Normalized Variable Diagram (NVD)

3.1.2.5. Viscous Fluxes

In order to calculate the viscous fluxes across a face *j*, we need to average the values of the flow variables between the neighbour cells as ,

(3.31) $$\vec{Q}_{IJ} = \frac{1}{2}\left(\vec{Q}_I + \vec{Q}_J\right)$$

And for a gradient,

(3.32) $$\nabla\vec{Q}_{IJ} = \overline{\nabla\vec{Q}_{IJ}} + \left[\overline{\nabla\vec{Q}_{IJ}} \cdot \vec{t}_{IJ} - \left(\frac{\partial\vec{Q}}{\partial l}\right)_{IJ}\right] \cdot \vec{t}_{IJ}$$

where $\boldsymbol{\tau_{ij}}$ is the unit vector pointing from cell center i to cell center j. The mean gradient is computed as shown bellow:

(3.33) $$\overline{\nabla\vec{Q}_{IJ}} = \frac{1}{2}\left(\nabla\vec{Q}_I + \nabla\vec{Q}_J\right)$$

And by using the finite difference method, the gradient across the line that passes through the cell centers will be also computed,

(3.34) $$\left(\frac{\partial\vec{Q}}{\partial l}\right)_{IJ} \approx \frac{\vec{Q}_J - \vec{Q}_I}{l_{IJ}}$$

At last, the gradient of the flow variables is calculated using the Green-Gauss theorem

(3.35) $$\nabla\overrightarrow{Q} \approx \frac{1}{\Omega}\int_{\partial\Omega}\overrightarrow{Q}_{Ik}\cdot\vec{n}\mathrm{d}S \ \ , k \in \mathcal{N}(i)$$

3.1.2.6. Temporal Discretization

In an implicit scheme, for every time true computational step, a pseudo-steady problem is solved. Let $\boldsymbol{Q}^*$ be the flow variables we need to solve the pseudo-steady problem and until it converges they are inconsistent with the original unsteady problem . At every pseudo-time step a (3.36) type system needs to be solved.

(3.36) $$\Gamma\frac{\partial\left(\overrightarrow{Q}^*\Omega\right)}{\partial\tau} + \overrightarrow{R}^* = 0$$

Where $\boldsymbol{R}^*$ stands for the unsteady residual defined as,

(3.37) $$\overrightarrow{R}^* = \overrightarrow{R}_\Omega\left(\overrightarrow{Q}^*\right) + \Gamma_e\frac{\partial\left(\overrightarrow{Q}^*\Omega\right)}{\partial t}$$

The solution of the original system is obtained when $\boldsymbol{R}^* \rightarrow \boldsymbol{0}$ and $\boldsymbol{U}^* \rightarrow \boldsymbol{U}^{n+1}$.

Discretizing the unsteady term at time level n+1, and writing the time derivative as a series expansion of successive levels backwards in time,

$$\frac{\partial\left(\overrightarrow{Q}\Omega\right)}{\partial t}=\frac{1}{\Delta t}\left[\varphi_{n+1}\left(\Omega\overrightarrow{Q}\right)^{n+1}+\varphi_{n}\left(\Omega\overrightarrow{Q}\right)^{n}+\varphi_{n-1}\left(\Omega\overrightarrow{Q}\right)^{n-1}+\varphi_{n-2}\left(\Omega\overrightarrow{Q}\right)^{n-2}+...\right] \tag{3.38}$$

The above equation can also be written as,

$$\begin{aligned}\frac{\partial\left(\overrightarrow{Q}\Omega\right)}{\partial t}=\frac{1}{\Delta t}\left[\overrightarrow{Q}^{n}\left(\varphi_{n+1}\Omega^{n+1}+\varphi_{n}\Omega^{n}+\varphi_{n-1}\Omega^{n-1}+\varphi_{n-2}\Omega^{n-2}+...\right)+\right. \\ \left.\varphi^{n+1}\left(\overrightarrow{Q}^{n+1}-\overrightarrow{Q}^{n}\right)\Omega^{n+1}+\varphi^{n-1}\left(\overrightarrow{Q}^{n-1}-\overrightarrow{Q}^{n}\right)\Omega^{n-1}+\varphi^{n-2}\left(\overrightarrow{Q}^{n-2}-\overrightarrow{Q}^{n}\right)\Omega^{n-2}+...\right]\end{aligned} \tag{3.39}$$

By introducing the Geometric Conservation Law (GCL),

$$\frac{d}{dt}\int_{\Omega(t)}\mathrm{d}\Omega=\oint_{\partial\Omega_{I}(t)}\vec{u}_{vol}\cdot\vec{n}\mathrm{d}S \tag{3.40}$$

and by using the finite volume method and discretising the unsteady term of GCL with the same sequence of the BDF scheme as in the (3.39)

$$\frac{1}{\Delta t}\left[\left(\varphi_{n+1}\Omega^{n+1}+\varphi_{n}\Omega^{n}+\varphi_{n-1}\Omega^{n-1}+\varphi_{n-2}\Omega^{n-2}\right)+...\right]=\overrightarrow{R}_{GCL}^{n+1} \tag{3.41}$$

Now the unsteady term can be written as,

$$\frac{\partial\left(\vec{Q}\Omega\right)}{\partial t}=\vec{Q}^{n}\vec{R}_{GCL}^{n+1}+$$

$$\frac{1}{\Delta t}\left[\varphi_{n+1}\left(\vec{Q}^{n+1}-\vec{Q}^{n}\right)\Omega^{n+1}+\varphi_{n-1}\left(\vec{Q}^{n-1}-\vec{Q}^{n}\right)\Omega^{n-1}+\varphi_{n-2}\left(\vec{Q}^{n-2}-\vec{Q}^{n}\right)\Omega^{n-2}+...\right] \tag{3.42}$$

The pseudo-steady term of equation (3.23) is discretised by first order backward difference scheme

$$\frac{\partial\left(\vec{Q}^{*}\Omega\right)}{\partial\tau}=\Omega^{n+1}\frac{\vec{Q}^{*,k+1}-\vec{Q}^{*,k}}{\Delta\tau}=\Omega^{n+1}\frac{\Delta\vec{Q}^{*,k}}{\Delta\tau} \tag{3.43}$$

Local Time Stepping

In order to facilitate convergence the local time stepping techique is used. The time step is determined by ,

(3.44)
$$\Delta\tau=CFL\frac{\Omega_{I}}{\left(\hat{\Lambda}_{c}+C_{s}\hat{\Lambda}_{v}\right)_{I}}$$

The convective spectral radii defined by,

(3.45) $$\left(\hat{\Lambda}_c\right)_I = \sum_{j=1}^{N_f} \left(\left(|\vec{v}_{Ij} \cdot \vec{n}_{Ij}| + c_{Ij} - \frac{V_g}{2} \right) \right) \Delta S_{Ij}$$

And the viscous spectral radii

(3.46) $$\left(\hat{\Lambda}_v\right)_I = \frac{1}{\Omega_I} \sum_{j=1}^{Nf} \left[2 \frac{(\mu_L + \mu_T)_{Ij}}{\rho_{Ij}} \right] (\Delta S_{Ij})^2$$

3.1.3.Turbulence Modeling

Regarding turbulence modeling, the k − ω SST model of Menter [12] is implemented. The k−ω SST model is based on the k−ε model and the simple k−ω model. It combines the positive aspect of these two models. To be more precise, at the boundary layer, the k−ω SST model shows the same behavior as the simple k−ω model. Because of this, no wall functions, approximations close to the wall, have to be applied. Outside this boundary layer, the k−ω SST model behaves like the k−ε model which makes it more robust than the simple k−ω model.

3.2. MESH CHARACTERISTICS AND MOTION

The mesh in the flow field is deforming, as the viscous wall (Barge) is moving (or deforming) . In each time-step, a new grid with updated nodal co-ordinates is required according to the Navier-Stokes equations solution for the specific moment of time. Regeneration of the grid for every time step can fulfill that requirement, but may not be efficient. For this type of problems, without inordinate grid distortion, mathematical algorithms can be developed to deform the grid according to the moving wall,while keeping the connectivity of the cells unchanged, using a distance function to decide the velocity vector for each node of the moving mesh.

As *Y.Zhao, J.Tai* and *F.Ahmed* proposed in their work [13] *"Simulation of micro flows with moving boundaries using high-order FV method on unstructured grids"* a general distance function will be used, consisting of two exponential damping functions. As they suggest, *the shortest distance of every node (is) to solid wall is measured as* ***d(is)*** *and the wall node that is closest to this inner node is also identified as iswall*. *A maximum of all* ***d(is)*** *is determined for non-dimensionalization* ***(dmax)***. To now determine the displacement of each node we will use the formulation,

$$\overrightarrow{dr}(is) = f(is)\overrightarrow{dr}(iswall)$$

where,

$$f(is) = \frac{ly^2(is)}{lx^2(is) + ly^2(is)}$$

where,

$$lx(is) = \frac{1 - \exp[-d(is)/dmax]}{(e-1)/e}$$

and,

$$ly(is) = \frac{1 - \exp[1 - d(is)/dmax]}{(1 - e)}$$

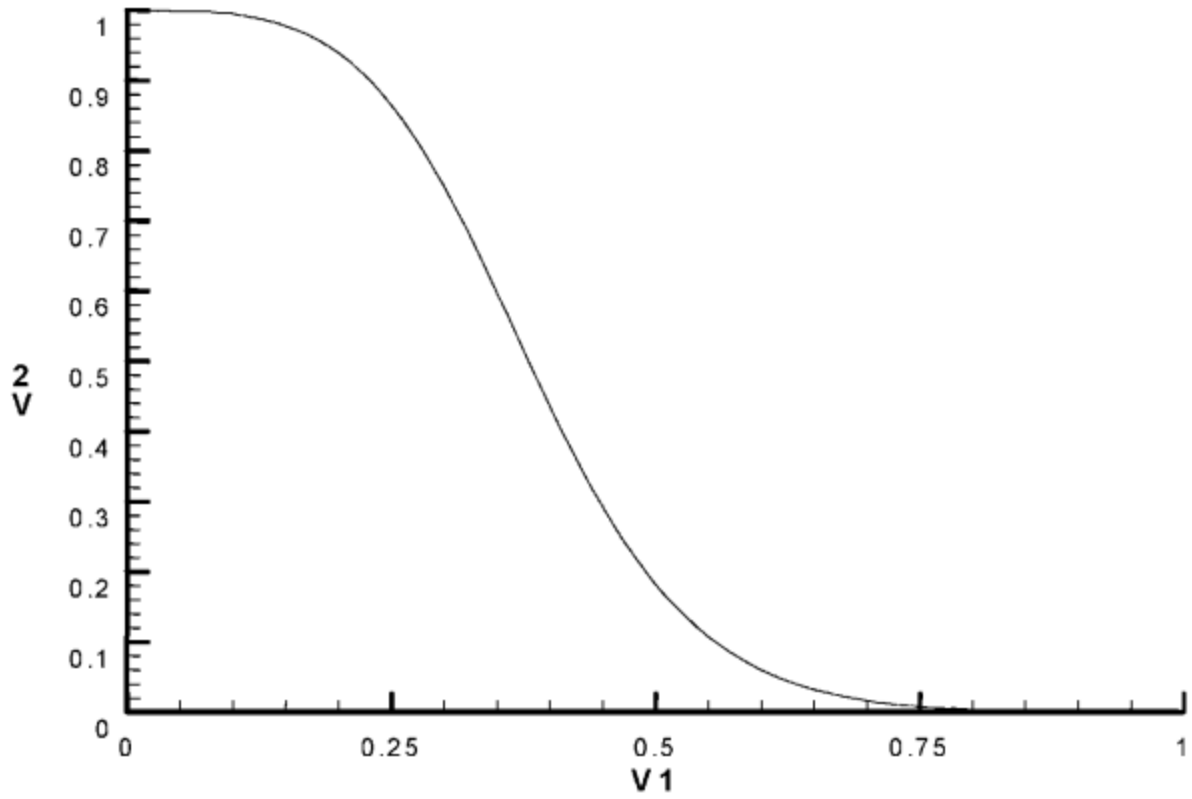

Figure 3.2 : *"Value of the distance function vs Non-dimensionalised distance"*

As it may have already been noticed, the distance function tends to 1 when ***d*** tends to zero and also ***f*** tends to zero when ***d*** tends to d_{max}. This property allows the grid to be rigid very far and very near from the wall, and elastic in between making it easy to be deformed. The variation of the values of the distance function with the non-dimensionalised distance is shown also in ***Fig.1***.

4. COMPUTATIONS

4.1 COMPUTATIONAL SPACE, BOUNDARY CONDITIONS AND MESHING

4.1.1.Numerical tank and simulation models

Irkal Mohsin A.R., S.Nallayarasu and S.K.Bhattacharyya et al. [15] in 2014 studied the roll motion and the damping of a 1-DoF 3-D barge model with (BK10) and without (BK00) bilge keels. Their study provided experimental data with which we can validate the accuracy of our numerical solver. The model's characteristics are presented in ***Table 1***.

Details	Values
Draft (*T*) (m)	0.12 m
Depth (*D*)	0.20 m
Breadth (*B*)	0.30 m
Length (*L*)	-
Bilge Radius	25 mm
Depth to Draft ratio (*D/T)*	1.67
Displacement ( )	20.88 kg
I	0.2244 kg-m^2
Kxx /B	0.346
BM	0.0625 m
KG	0.08 m
GM	0.0425 m

Table 1*: "Experimental model characteristics"*

To transfer the same characteristics in our model in the 2-D approach, corrections were made in order for the moment of inertia (I) to be consistent with the physical problem.

The numerical tank that was used is shown in ***Figure 4.1(a)*** along with the barge and the free surface. The length of the tank is set L_{TANK}=12 m and the height H_{TANK}=2.5 m. The position of the free surface is set at y_{fs}=0.6 m , measuring from the bottom of the tank. In order for the radiated waves, generated by the rolling barge not to be reflected in the solid walls, damping zones are set at positions x_{d1}=-5.0 m and x_{d2}=5.0 m to absorb the wave energy. The bilge keel's characteristics are well presented in ***Figure 4.1(b)***, and also placed in ***Table 2***.

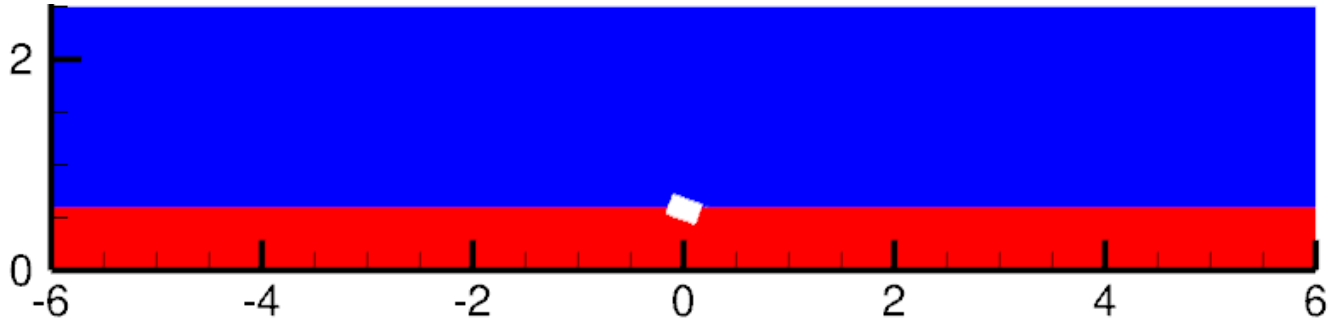

Figure 4.1(a): Numerical Tank

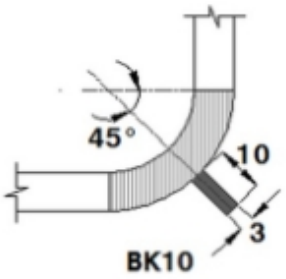

*Figure 4.1(b)**:** BK10 Bilge keel's dimensions and characteristics*

Bilge keel dimensions	BK00	BK10
Width(b) in mm	0	10
Width to beam ratio (b/B)	0	0.033
Angle with horizontal ( )	-	45^0

Table 2 :*"Bilge keel's details"*

4.1.2. Boundary Conditions

The boundary conditions that were applied at each solid boundary of our numerical tank are shown in **Table 3,** and will be discussed in this paragraph. At the solid boundaries of the Barge a "*Viscous Wall*" condition was applied. The *Viscous Wall* condition is expressed mathematically by the No Slip equation which will be discussed in the next paragraph. Faces AB, BC and CD where treated as "*Farfield"* to deal with the hyperbolic character of the problem of the flow at infinite distance from a rotating body. To ensure that no wave energy is reflected and reinserted in the computational field damping zones are set at positions near faces AB, CD and so the importance of the *Farfield* condition at each of these faces is reduced. The remaining face of the tank AD, was considered a *"Wall"*. A brief presentation of the equations applied is provided in the following paragraph as Papadakis [15] proposes.

4.1.2.1. Wall Boundary Conditions

- ***Inviscid Wall***

The fluid is considered inviscid on solid boundaries,

$$(\vec{u} - \vec{u}_g) \cdot \vec{n} = 0 \qquad (4.1)$$

Where U_g denotes the grid velociy. Density and pressure are set equal to their values at the cell center next to the wall,

$$p_w = p_I,\ \rho_w = \rho_I \qquad (4.2)$$

- ***Viscous Wall***

In the general case the fluid is viscous and the no slip wall condition is applied,

(4.3) $$\vec{u} = \vec{u}_g$$

Density and pressure are treated as in the inviscid case. Regardless the assumptions made for the fluid, the convective fluxes take the form,

$$\vec{F}_{cwall} = \begin{pmatrix} 0 \\ n_x p_w \\ n_y p_w \\ n_z p_w \\ p_w V_g \end{pmatrix} \qquad (4.4)$$

Where, $$V_g = \vec{u}_g \cdot \vec{n}$$

4.1.2.2. Far-field Boundaries

As said, at the far-field it is important to be consistent with the hyperbolic character of the problem.

Face	***Boundary Condition***
Ceiling	*Farfield*
Sides	*Farfield-Damping Zones*
Bottom	*Wall*
Barge	*Viscous Wall*

Table 3 :"*Boundary conditions by face****"***

4.1.3. Meshing

For the generation of the mesh, Beta ANSA software was used. A structured mesh of quads (mainly) was generated around the rolling barge along with a zone lengthwise to the free surface. The rest of the domain was set unstructured covered also by quads. The most sensitive grid area was the part of the domain around the bilge keel in which bigger precision was needed. A picture of the meshing in the bilge keel area is shown in ***Fig.4.2.1.***

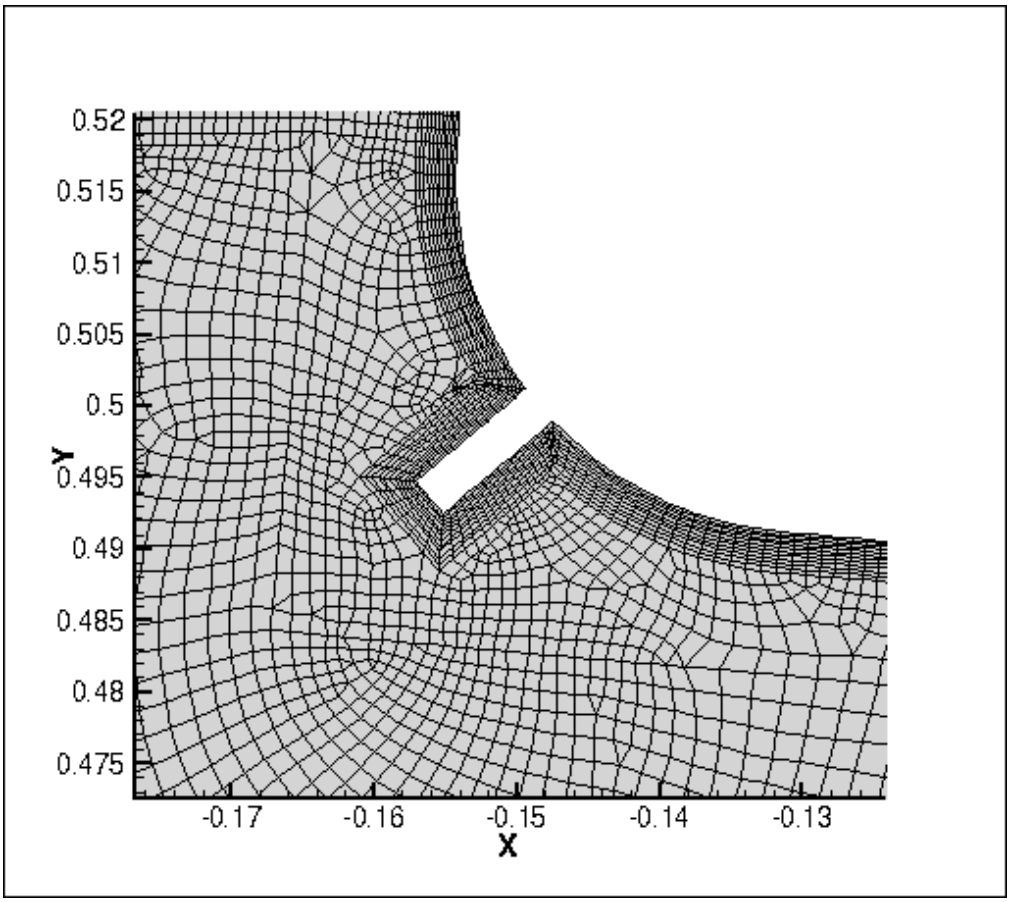

Figure 4.2.1: Meshing Around the Bilge Keel

4.2. MESH SENSITIVITY STUDY

4.2.1. Mesh Convergence

For our study 3 grid cases were examined to determine whether mesh convergence is reached and when. Images of the meshing around the rolling barge for each case are shown in ***Fig 4.3.1*** .The 3 different mesh refinements along with the simulation's time are given in ***Table 4*** . A 5 degree initial angle free decay simulation is performed for each one , the 3 resulting curves along with the experimental free roll decay curve are shown in ***Fig.4.3.2*** .

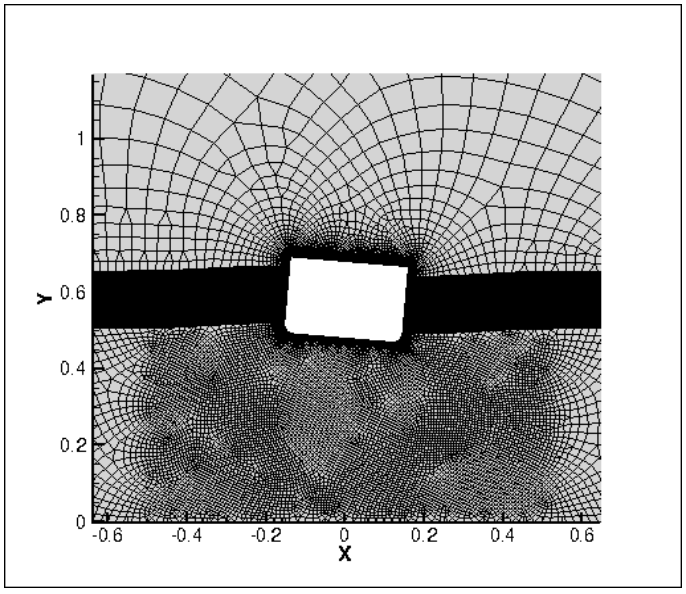

Figure 4.3.1 (a): Coarse

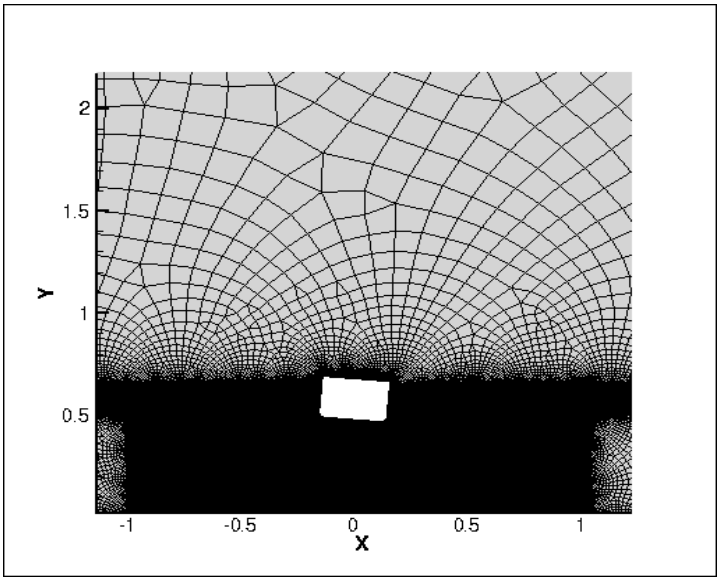

Figure 4.3.1 (b): Medium

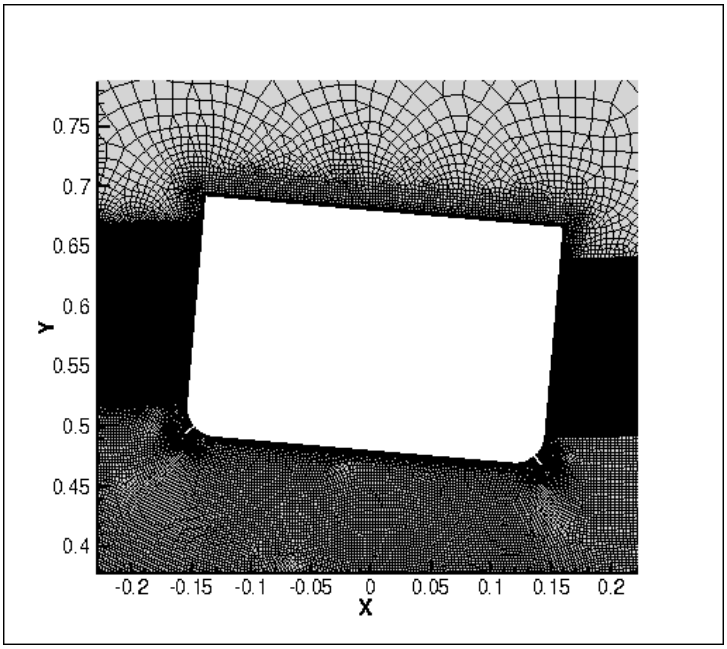

Figure 4.3.1 (c): Fine

The 3rd column of Table 4 refers to the total time *MaPFLow* needs to perform 16 roll cycles .

Mesh	***Number of Cells (Approximately)***	***Simulation's time***
Coarse	*110,000*	*14.31h*
Medium	*330,000*	*15.99h*
Fine	*570,000*	*26.06h*

***Table 4**: "Mesh Characteristics"*

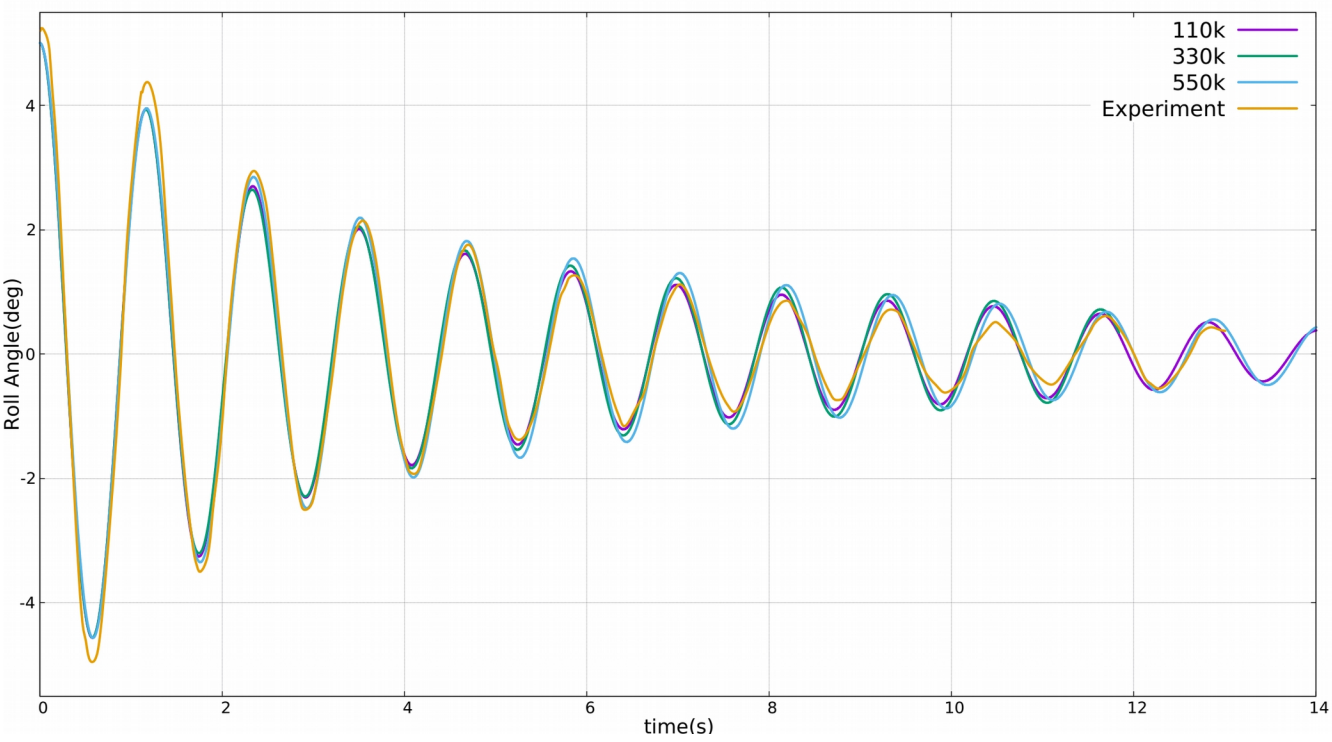

Figure 4.3.2(a) : Mesh Independence Study

Zooming in the 8th peak (***Figure 4.3.2(b)***) of the simulations it can be observed that the deviation between coarse and medium mesh simulations is noticeably more significant than the deviation between medium and fine. As a result we can assume our responses converge and so our solution is mesh independent.

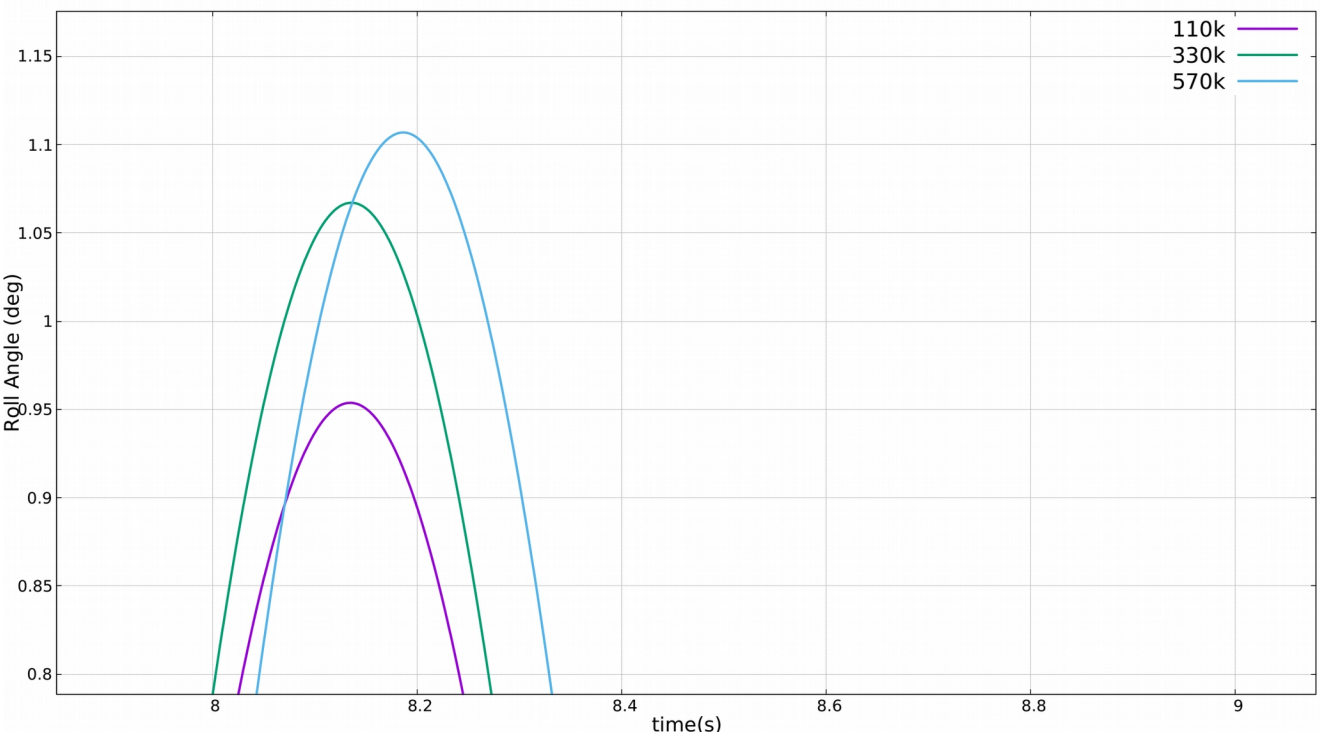

Figure 4.3.2(b) : Mesh independence study zoom

4.2.2. Time-step Independence Study

Along with the mesh sensitivity analysis a time-step sensitivity study was also concluded. Using a coarse-medium mesh (~185k cells) , 3 simulations were performed as shown in ***Table 5***. The time history of the simulations is shown in ***Fig. 4.3.3*** .

Time-step(T/*)	***Time-step(s)***	***Color***
T/400	*0.0028*	*Blue*
T/800	*0.0014*	*Green*
T/1600	*0.0007*	*Magenda*

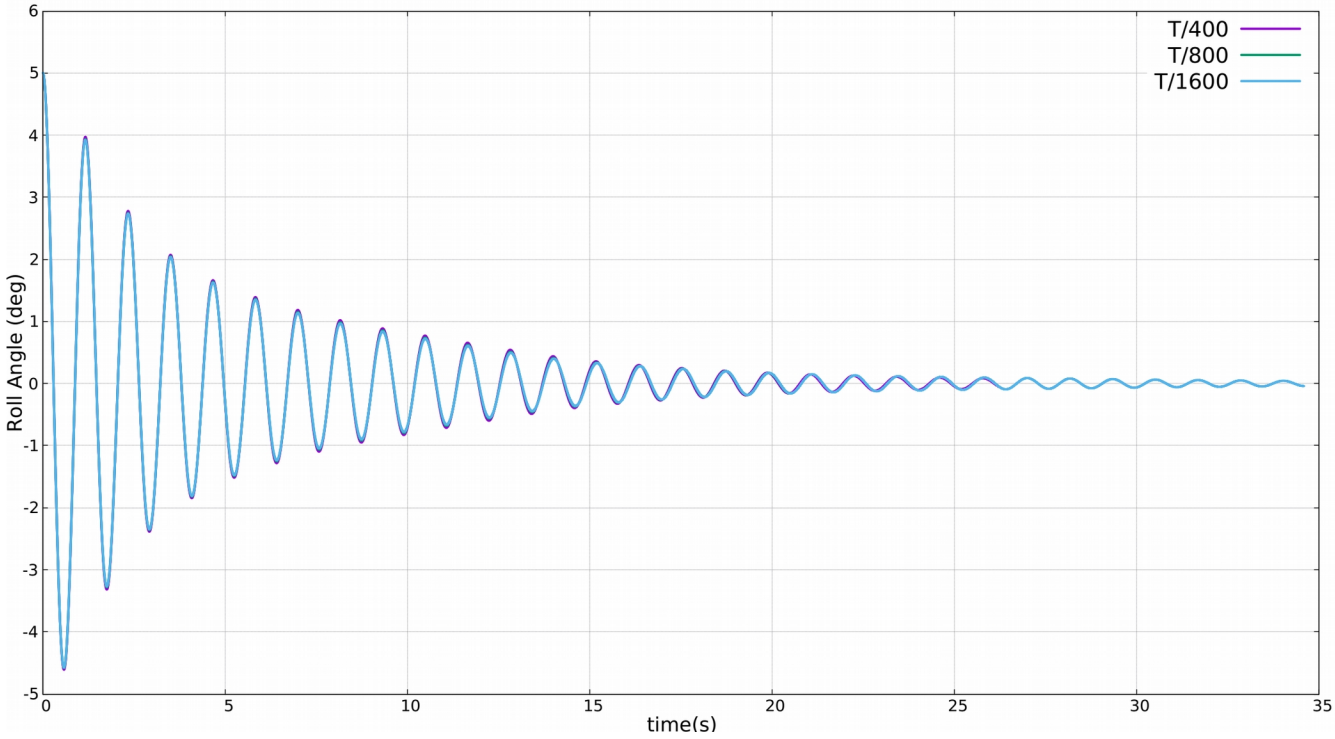

Figure 4.3.3: Time-step Convergence

As it can easily be noticed the roll responses of the simulations, under each one of the time-step cases, are really similar and no significant deviation is observed. The solution MaPFlow produces is considered time-step independent.

4.3. FREE ROLL DECAY TESTS

4.3.1.Validation Approach

In order to ensure that the simulation results obtained by *MaPFlow* are reliable we had to validate them with experimental data performed by Irkal Mohsin A.R., S.Nallayarasu and S.K.Bhattacharyya for the Indian Institute of Technology, Madras in 2014. In their work [14] "*Experimental and CFD Simulation of Roll Motion of Ship with Bilge Keel*" they provide free roll decay experimental results with which we will validate the accuracy of our numerical solver. Furthermore, in their work "Numerical Prediction of Roll Damping of Ships with and without Bilge Keel" forced roll ,under wave excitation, tests were performed and their respective curves were extracted with which we will compare our forced roll simulations results .

At this point of our investigation we will validate whether our free decay simulations, with (BK10) and without (BK00) bilge keel, are consistent with the experimental results Irkal Mohsin A.R., S.Nallayarasu and S.K.Bhattacharyya provide. So, at an initial angle of 20 degrees :

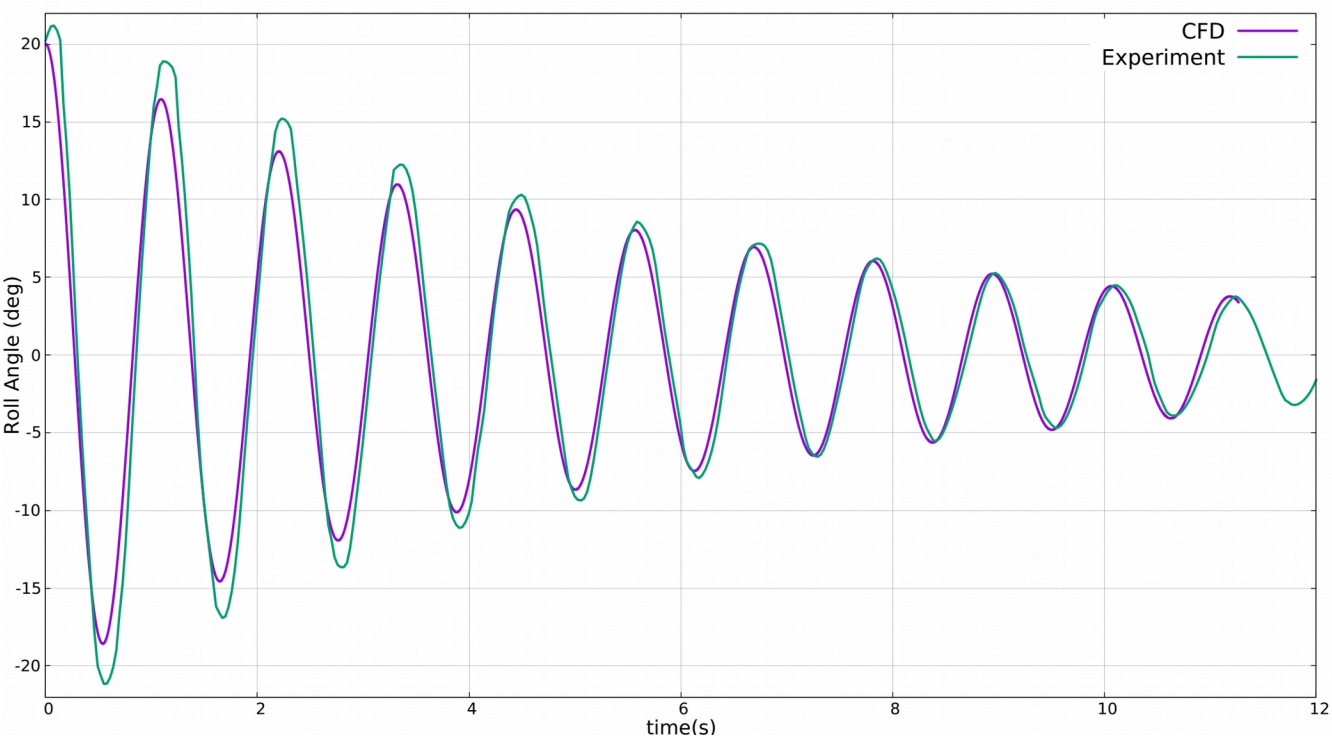

Figure 4.4.1(a): BK00 free roll decay at a 20 degree initial angle

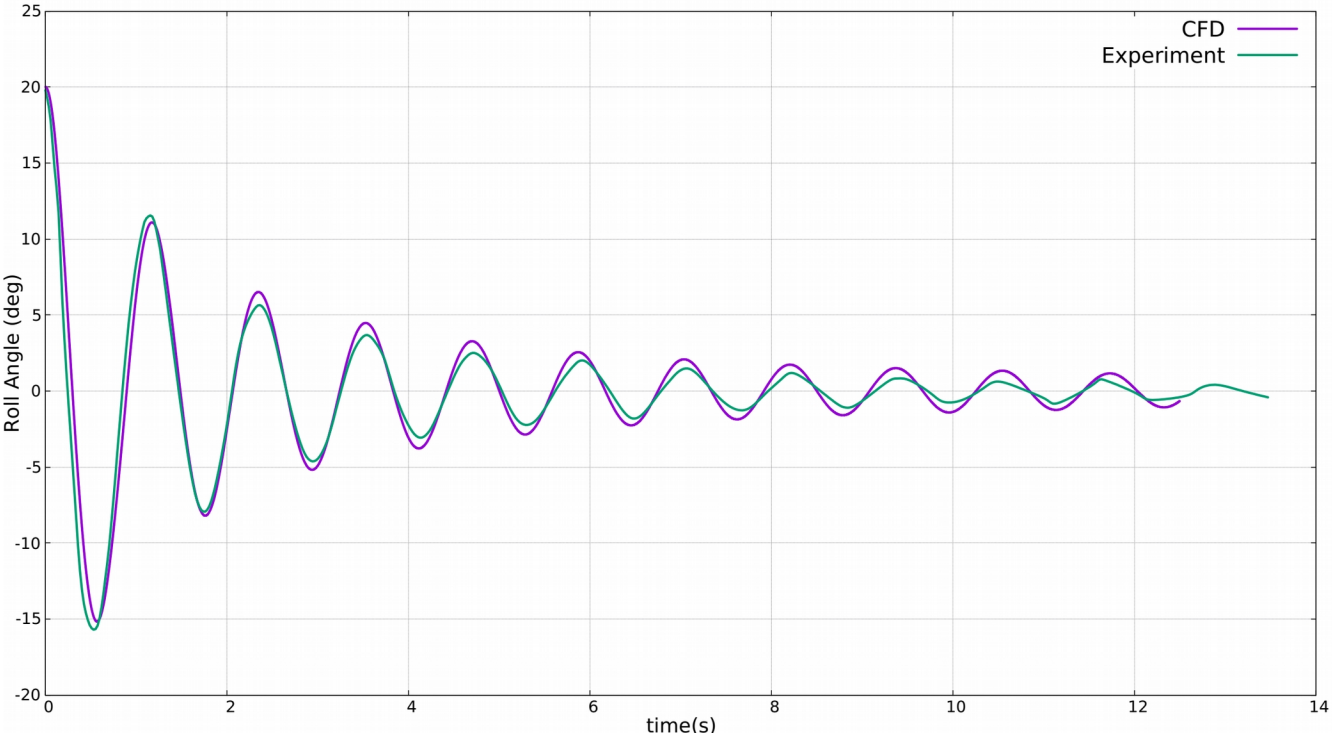

Figure 4.4.1(b): BK10 free roll decay at a 20 degree initial angle

The respective free roll decay curves of BK00 and BK10 at a 5 degree initial angle are shown in ***Fig.4.4.2*** :

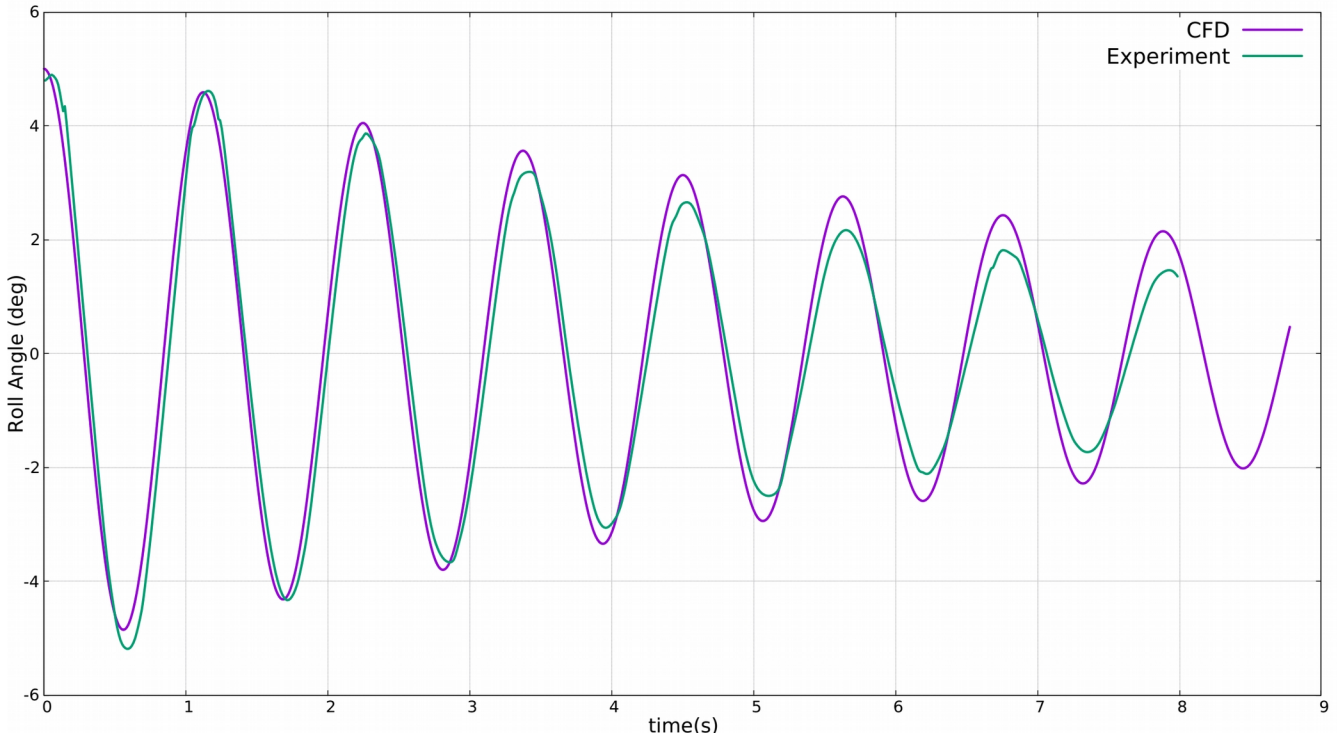

Figure 4.4.2(a): BK00 free roll decay at a 5 degree initial angle

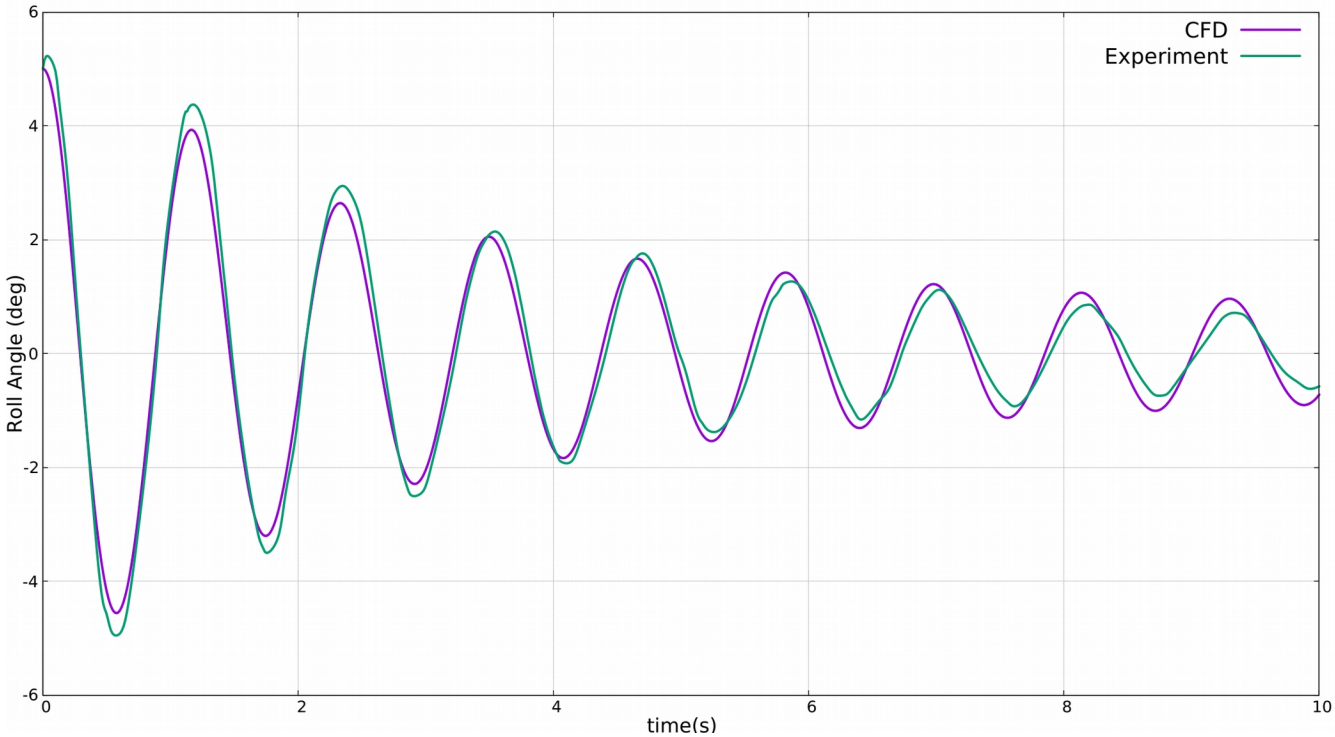

Figure 4.4.2(b): BK10 free roll decay at a 5 degree initial angle

As it can clearly be noticed the largest deviations are observed in the simulations of BK00 as the roll angle reaches values lower than 3.5-4 degrees. Assuming that in such low roll angles the damping is expected to be mainly linear, we will look for causes of deviations straight at the radiated waves of the rolling barge (BK00) , comparing them with the experimental measurements provided by Irkal [16]. At a position 0.5 m away from BK00 we place a station to measure the free surface elevation during the rolling which is shown in ***Fig.4.4.3(a)***.

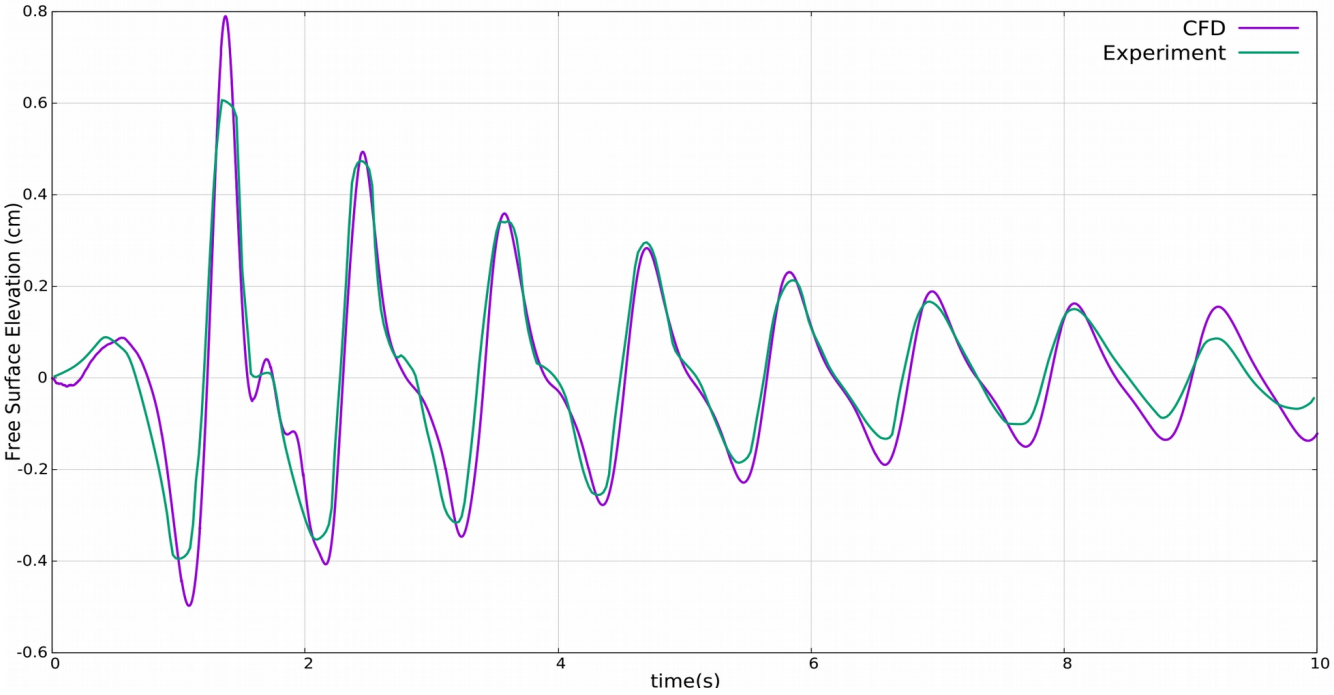

Figure 4.4.3(a): Radiated Wave Caused by the Rolling of BK00 : 20 degrees initial angle simulation

Looking at ***Fig.4.4.3(a)*** we see good agreement between our results and the experiment. Although some elevation peaks may differ from experiment to CFD the form of the curves is pretty much similar. Assuming that the linear damping is sufficiently calculated in our simulations we are now led to the conclusion that the main cause for the deviations observed is the loss of information between the 3D experiments and the 2D simulations. The lack of modeling of the tunnel, along with the 3D flow phenomena that accompany it seem to be the main reason why there is no perfect agreement between experiment and CFD.

In the next figure is presented the radiation of BK10 when rolling, also starting at a 20 degrees initial angle.

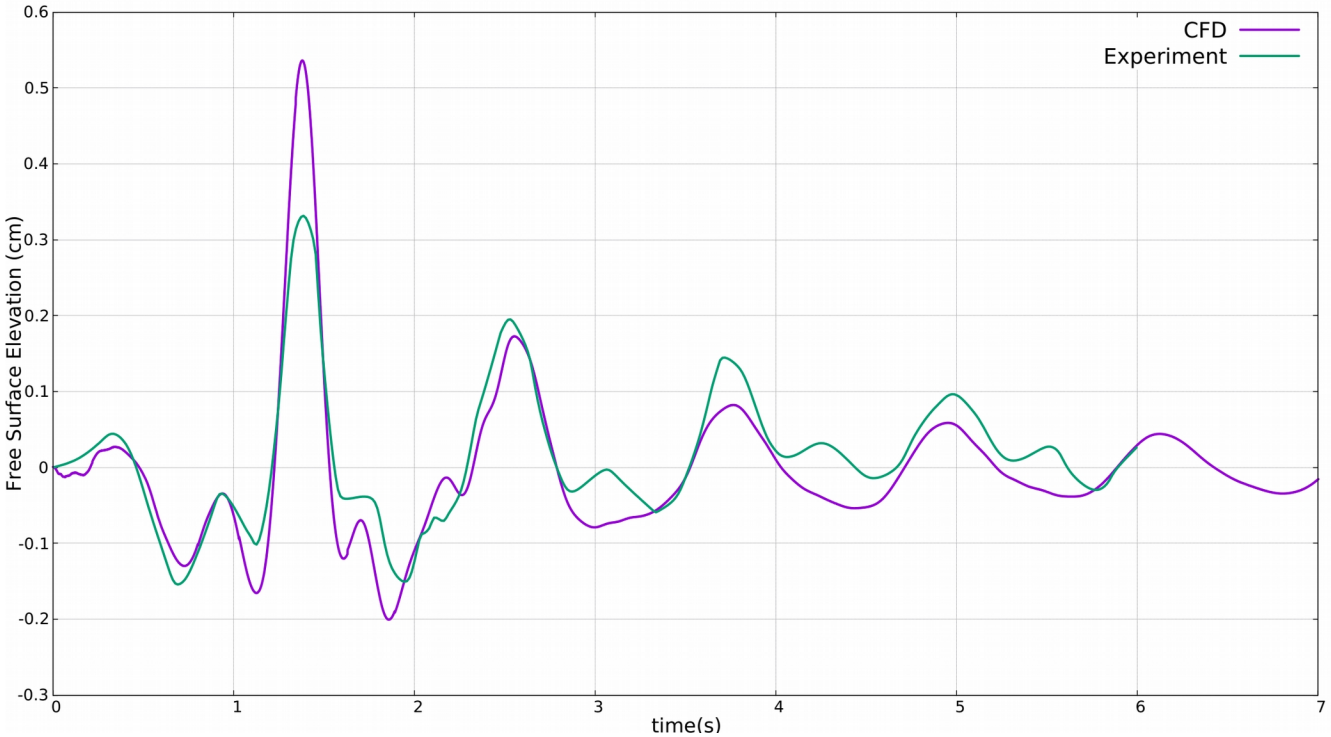

Figure 4.4.3(b): Radiated Wave Caused by the Rolling of BK10 : 20 degrees initial angle simulation

It can be seen that the amplitude of radiated wave decreases with the attachment of bilge keels. This implies, the radiated waves's contribution in total roll damping decreases with the attachment of the bilge keels and as a result the contribution of viscous damping increases drastically.

4.3.2 Effect of the Bilge Keel on the vorticity field

At this point, we can observe how the vorticity field is affected by the bilge keel. Using a medium coarse grid (~180,000 cells) which was constructed in beta ANSA we will capture the vorticity under the hull caused by the barge's rolling at several moments of time. So in ***Fig.4.4.4*** ,

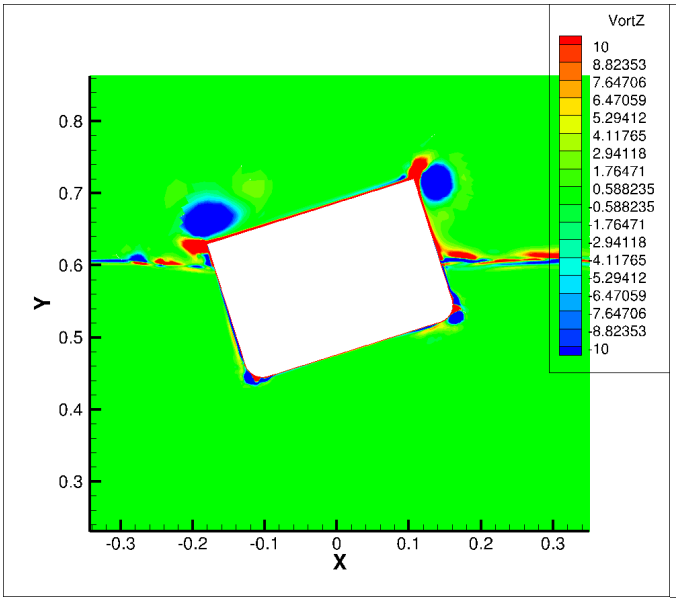

Figure 4.4.4(a): BK00 Vorticity field at t~0.5T

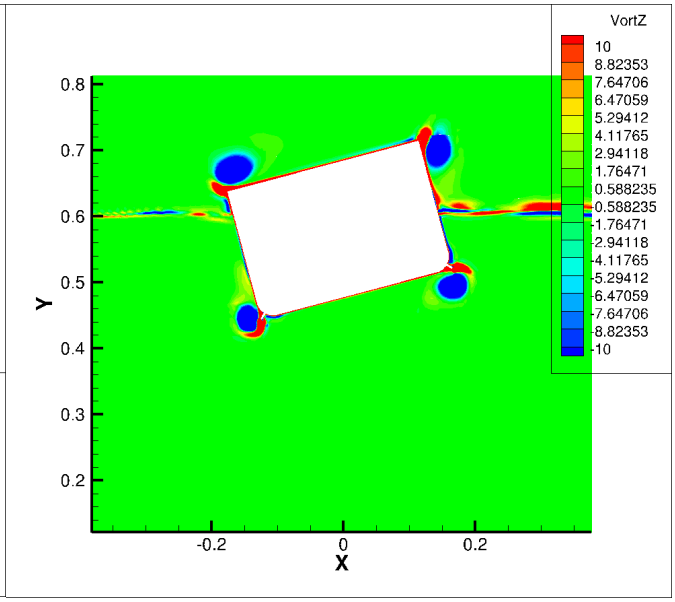

Figure 4.4.4(b): BK10 Vorticity field at t~0.5T

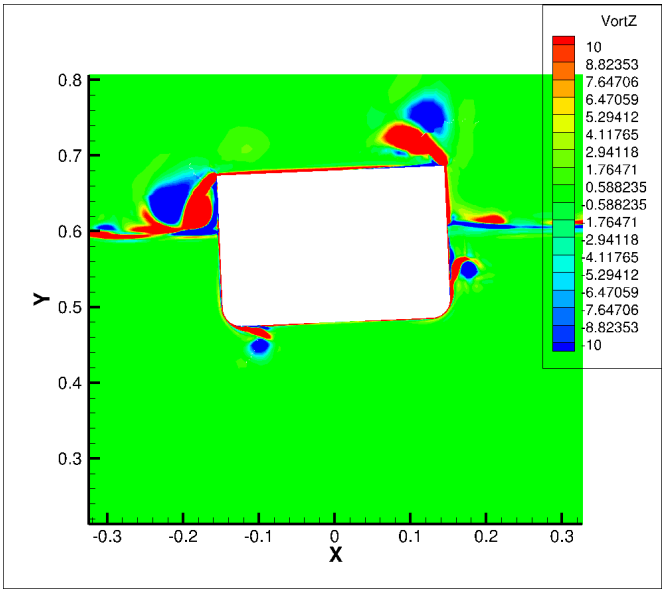

Figure 4.4.4(c): BK00 Vorticity field at t~0.75T

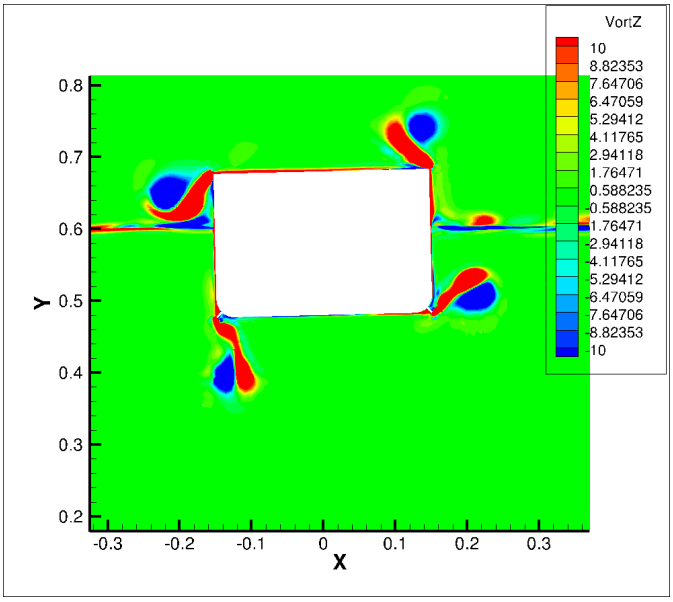

Figure 4.4.4(d): BK10 Vorticity field at t~0.75T

4.3.3.Calculating the Damping Coefficients

For the determination of the damping coefficients of the free roll decay system we used 4 free roll simulations performed at a medium-coarse grid (~180,000 cells), taking in consideration both linear and non linear roll models.

Linear damping calculation

The linear roll model that was considered in the analysis below is ,

$$(I + A)\ddot{\varphi} + B_l\dot{\varphi} + C\varphi = 0 \quad (4.5)$$

Using the equation (4.5) to model the free roll motion of BK00 and BK10, the damping ratio of the system, which describes the non-dimensional damping, is calculated using the expression (4.6) as Spyrou [17] suggests.

$$\zeta = -\frac{1}{\pi}\ln\frac{A_{\frac{1}{2}}}{A_0} \quad (4.6)$$

- **Damping ratio and natural period for a 5 degree initial angle free roll case**

5 degree initial angle free decay	*BK00*		*BK10*	
	Experiment	*CFD*	*Experiment*	*CFD*
Tn(s)	*1.113*	*1.127*	*1.181*	*1.175*
ζ	*0.027*	*0.025*	*0.051*	*0.0415*

Table 6: *Results of the 5 degree initial angle simulations*

- **Damping ratio and natural period for a 20 degree initial angle free roll case**

20 degree initial angle free decay	*BK00*		*BK10*	
	Experiment	*CFD*	*Experiment*	*CFD*
Tn	*1.114*	*1.117*	*1.196*	*1.175*
ζ	*0.033*	*0.029*	*0.077*	*0.065*

Table 7: *Results of the 20 degree initial angle simulations*

Calculating the mean values of *Tn*, *ζ* we can now observe a slight underestimation of *ζ* and a small period shift between CFD and Experimental results especially when adding a bilge keel. This may be caused by 3D effects not taken in consideration by our 2D simulations, as previously mentioned, or experimental systematic errors, such as the existence of friction between the barge and the solid axis the body rolls around. In the next paragraph an analysis is provided to show the development of *ζ* throughout the course of the simulations. In ***Figure 4.5.1*** the *ζ* coefficient is calculated at every semi-cycle of the free roll (calculating the damping ratio between oscillation's peaks) and so $\varphi_m = (\varphi_i + \varphi_{i+1})/2$ where φ_i are the roll angle peaks occurring during the oscillation. Observing the results, as said, a slight underprediction of the damping is noticed and for that reason six more simulations were performed to check whether the deviations remain constant for the various initial angle cases . In ***Figure 4.5.2*** the results for the damping ratio of the respective simulations are presented.

Expecting the roll damping to be mainly linear in a 5 degree initial angle roll simulation, we can now calculate the impact of the bilge keels in the damping ratio. More precisely, when adding the bilge keels, the damping ratio of our simulation increases to the 166% of the naked hull's damping ratio, compared to the 188,9% that is expected from the experimental results [14].

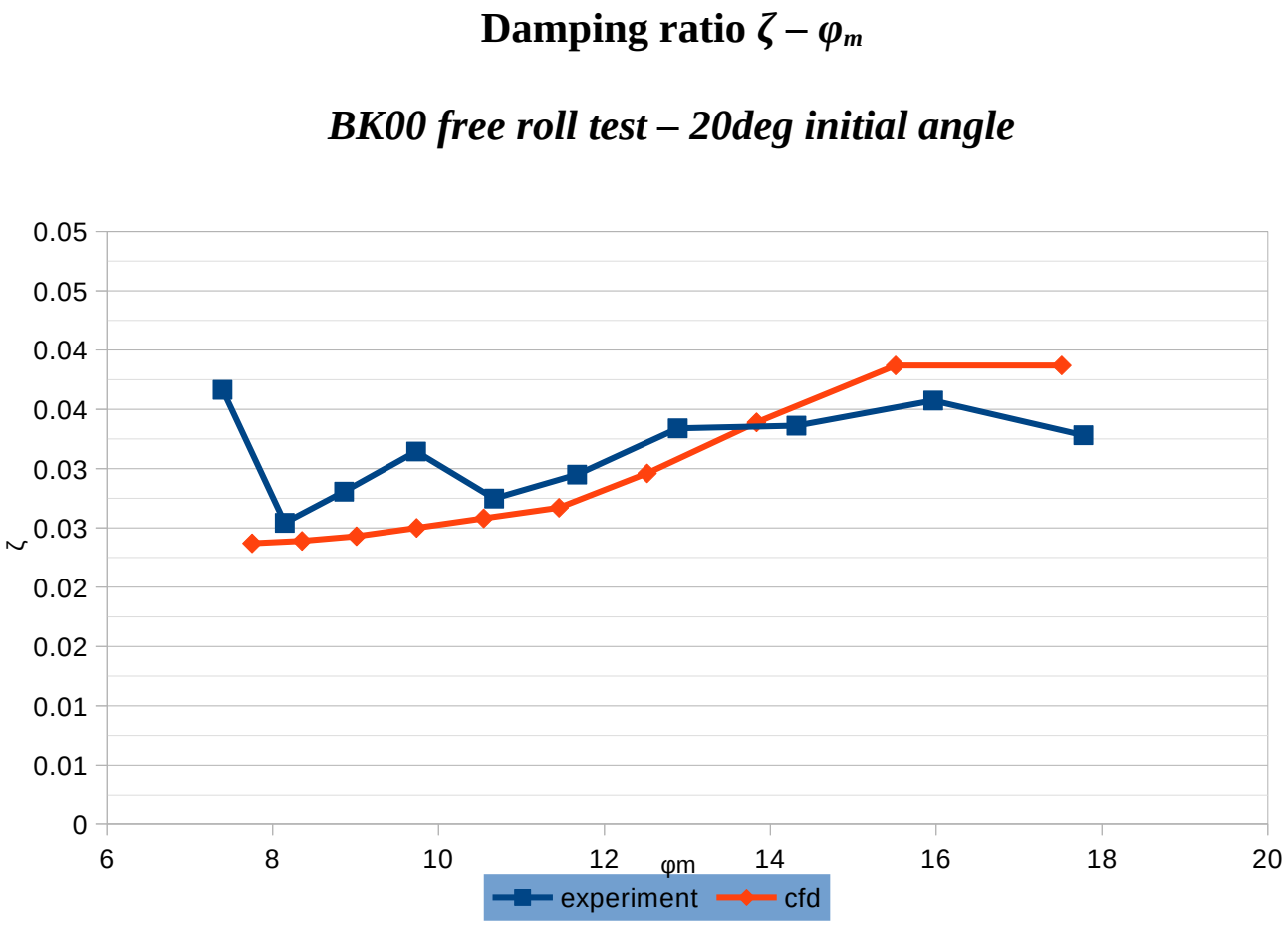

Figure 4.5.1(a) : ζ variation throughout roll motion for BK00 starting at a 20 degree initial angle.

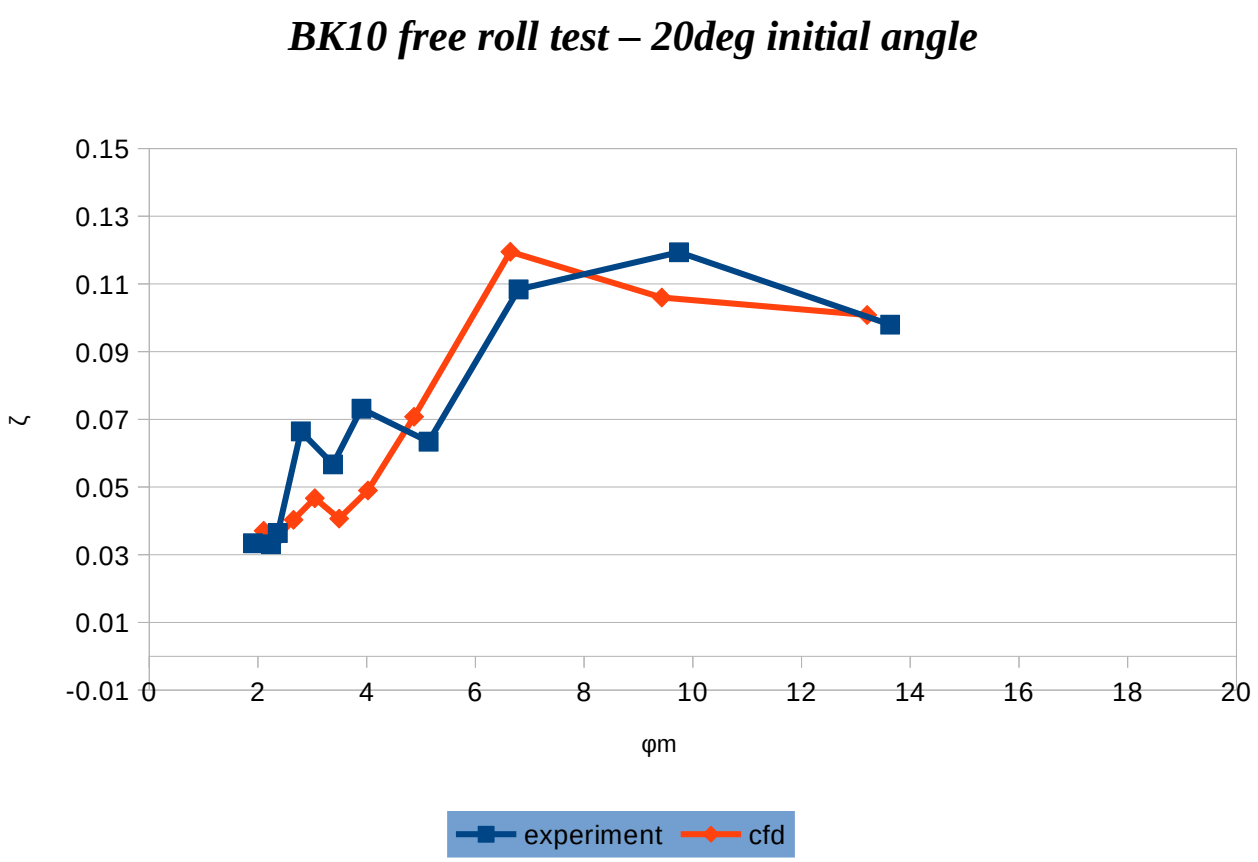

Figure 4.5.1(b) : ζ variation throughout roll motion for BK10 starting at a 20 degree initial angle.

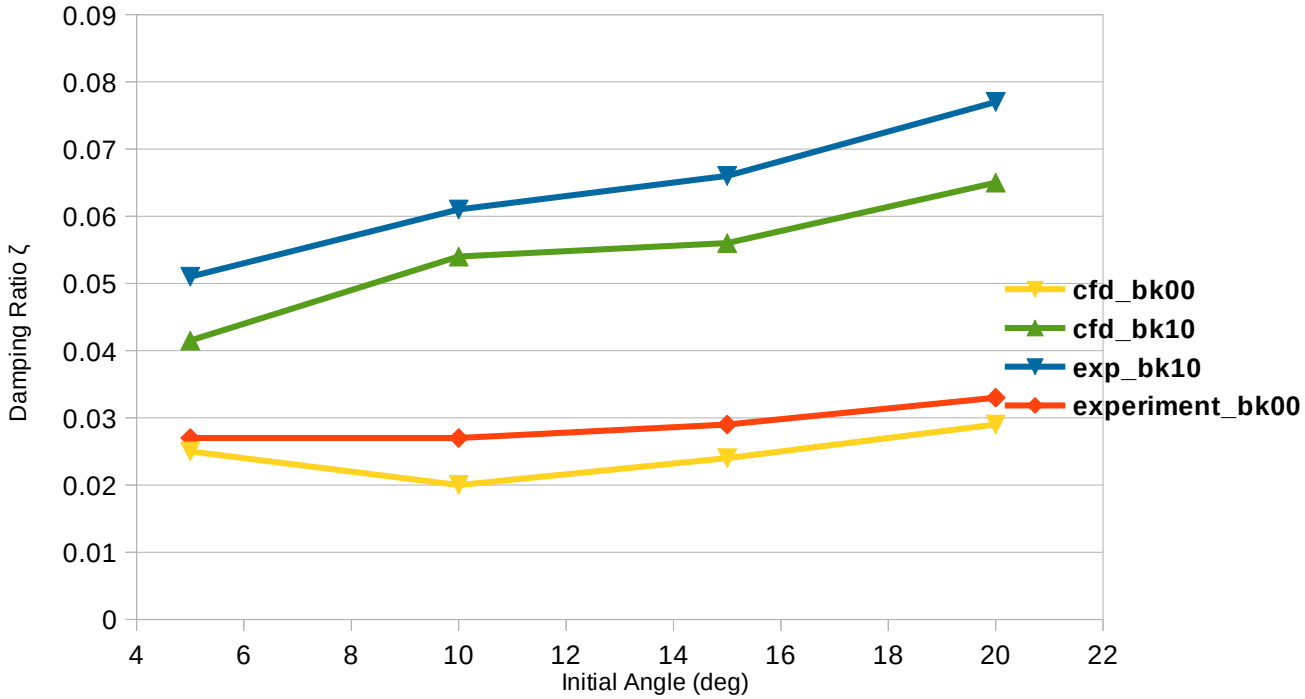

Figure 4.5.2: Damping Ratio Variation to Initial Angle

Figure 4.3.6. reveals that the damping ratio of the free decay system increases (in most cases) as the initial angle gets higher , thing we expected looking back at previous work done in the field [16]. The measurements refer to the first 8-10 cycles of the oscillation which is sufficient for accurate estimation of damping. The results concerning ζ , performed by *MaPFLow* are also summarized in ***Table 8***.

BK00		*BK10*	
Initial Angle	ζ	*Initial Angle*	ζ
5^o	0.025	5^o	0.042
10^o	0.020	10^o	0.054
15^o	0.029	15^o	0.056
20^o	0.033	20^o	0.065

Table 8 : *Damping ratio variation to Initial Angle*

Non-linear Damping calculation

The non-linearities increase and become sufficiently strong when adding a bilge keel and so a non linear damping analysis had to be developed for those cases. As S.A.W. Smaal proposes in his work [18] *"Roll Damping prediction: To determine linear and non linear damping coefficients based on multiple 2D CFD simulations"* the linear and higher order damping coefficients can be calculated from the decay curve. The roll model that is considered for this study is described by equation (4.7) ,

$$(I + A)\ddot{\varphi} + B_1\dot{\varphi} + B_2\dot{\varphi}|\dot{\varphi}| + C\varphi = 0 \tag{4.7}$$

In the ***Figure 4.5.3*** a typical decay curve is presented. A peak and its successive peak are given by x_n and x_{n+1} at time t_n and t_{n+1} respectively. The loss of energy in this interval is found using Equation (4.8)

$$\Delta E_n = \Delta E_{\text{kin},n} + \Delta E_{\text{pot},n} = \frac{1}{2}m\dot{x}_n^2 - \frac{1}{2}m\dot{x}_{n+1}^2 + \frac{1}{2}cx_n^2 - \frac{1}{2}cx_{n+1}^2 \tag{4.8}$$

Where ΔE is the difference in total energy, ΔE_{kin} is the difference in kinetic energy, ΔE_{pot} is the difference in potential energy, m is the mass, $\dot{x}$ is the velocity, c is the damping coefficient and n is a certain peak in the decay curve. At the peaks the velocity is equal to zero, this means that at time t_n and t_{n+1} , $\dot{x}_n = \dot{x}_{n+1} = 0$. If we apply this to Equation (4.8), eq. (4.9) is produced:

$$\Delta E_n = \frac{1}{2}c\left(x_n^2 - x_{n+1}^2\right) = \frac{1}{2}c\left(x_n + x_{n+1}\right)\left(x_n - x_{n+1}\right) = c\overline{x}_n\Delta x_n \tag{4.9}$$

Where $\overline{x}_n$ and Δx_n are defined as:

$$\overline{x}_n \equiv \frac{1}{2}\left(x_n + x_{n+1}\right) \tag{4.10}$$

(4.11) $$\Delta x_n \equiv x_n - x_{n+1}$$

From the general solution of a lightly (sub-critically) damped mass-damper-spring system, which a free roll decay test is, it results that:

$$c \approx m\omega^2 \qquad (4.12)$$

Using this and the definition of $\bar{x}_n$ and Δx_n , Equation (4.9) can now be written as Equation (4.13):

(4.13) $$\Delta E_n = m\omega^2 \bar{x}_n \Delta x_n$$

The work done by the damping force at ***n*** is given by (4.14):

$$W_{\text{damp},n} = \int_{t_n}^{t_{n+1}} \left(b_l + b_q|\dot{x}(t)|\right)\dot{x}(t)\dot{x}(t)\mathrm{d}t = b_l \int_{t_n}^{t_{n+1}} \dot{x}^2(t)\mathrm{d}t + b_q \int_{t_n}^{t_{n+1}} |\dot{x}(t)|\dot{x}^2(t)\mathrm{d}t$$

Where W_{damp} is the work done by the damping force, b_l (B_1) is the linear damping coefficient and b_q (B_2)is the quadratic damping coefficient. It is assumed that, within the time interval between t_n and t_{n+1} the roll angle is approximated by:

(4.15) $$x(t) = \bar{x}_n \cos\omega t$$

The corresponding roll velocity will then be:

(4.16) $$\dot{x}(t) = -\omega \overline{x}_n \sin \omega t$$

Substituting this velocity in Equation (4.14) gives:

(4.17) $$W_{\text{damp},n} = \omega^2 \overline{x}_n^2 b_l \int_{t_n}^{t_{n+1}} \sin^2 \omega \text{td}t + \omega^3 \overline{x}_n^3 b_q \int_{t_n}^{t_{n+1}} |\sin \omega t| \sin^2 \omega \text{tdt}$$

Solving this gives the total work done by the damping force:

$$W_{\text{damp,n}} = \pi \omega \overline{x}_n^2 b_l + \frac{8}{3} \omega^2 \overline{x}_n^3 b_q \qquad (4.18)$$

Assuming that all lost energy is caused by the damping force, it can be stated that:

(4.19) $$\Delta E_n = W_{\text{damp},n}$$

Using Equations (4.13) and (4.18), Equation (4.20) is obtained:

(4.20) $$m\omega^2 \overline{x}_n \Delta x_n = \pi \omega \overline{x}_n^2 b_l + \frac{8}{3} \omega^2 \overline{x}_n^3 b_q$$

Dividing Equation (4.20) by $\bar{x}_n^2$ and $m\omega^2$ gives Equation (4.21).

$$\frac{\Delta x_n}{\bar{x}_n} = \frac{\pi}{m\omega} b_l + \frac{8}{3m} b_q \bar{x}_n \tag{4.21}$$

The above expression can also be written as,

$$\frac{\Delta x_n}{\bar{x}_n} = p + q\bar{x}_n \tag{4.22}$$

Where,

$$b_l = \frac{p}{2\pi} b_{\text{crit}} \quad , \quad b_q = \frac{3q}{16\omega} b_{\text{crit}} \tag{4.23}$$

Plotting the difference in succeeding peaks against the average values of those two peaks for the complete decay curve and fitting a linear function through these points makes it possible to determine the values of ***p*** and ***q*** as the expression (4.22) suggests. In ***Table 9*** the ***p*** and ***q*** values are shown, in relation with the initial angle, for the respective cases examined.

Table 9 : *p – q analysis results*

BK10	***p***	***q***
5 DEG	*0.0833*	*0.0193*
20 DEG	*0.0808*	*0.0234*

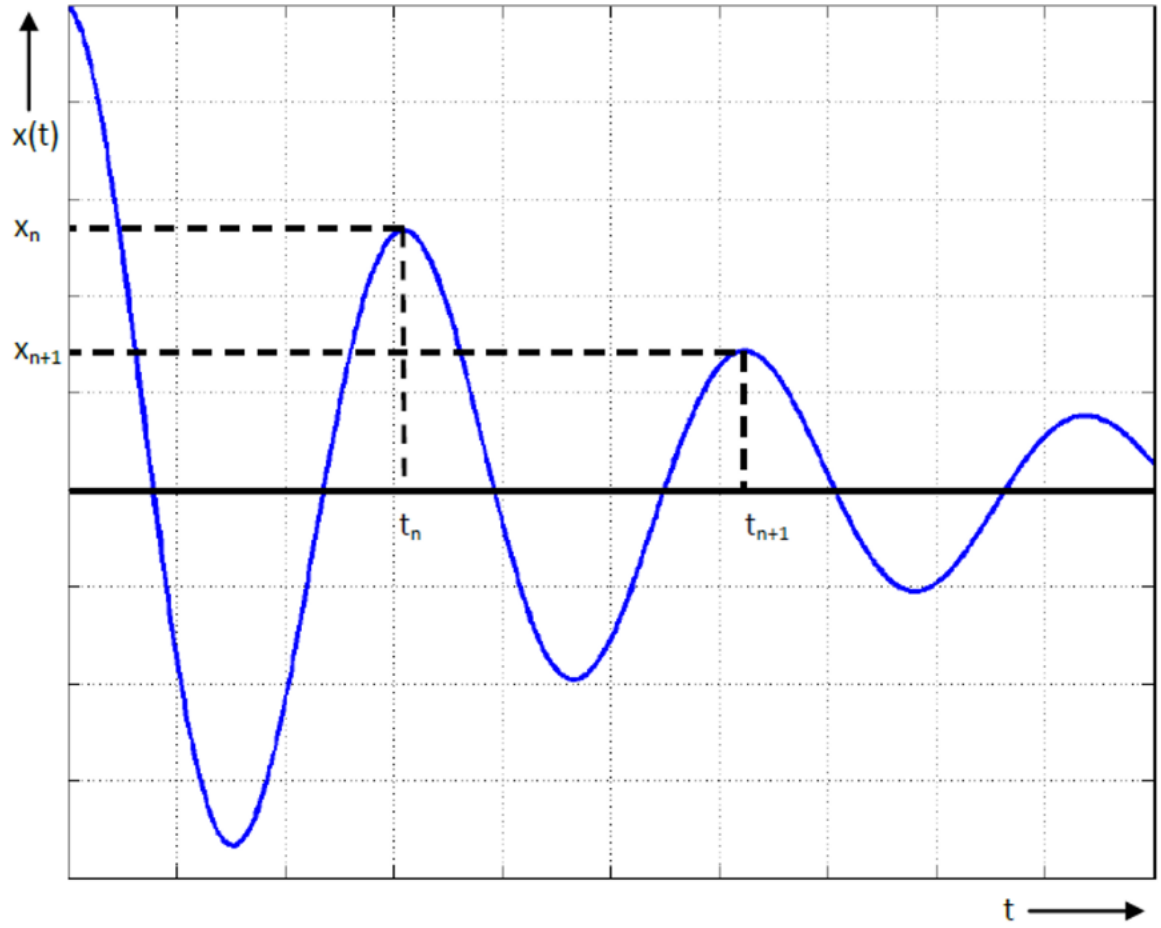

Figure 4.5.3: Free Roll Decay Typical Curve

In ***Figure 4.6.1*** the results of the above $p - q$ analysis are presented. The blue polyline represents the variation of the loss of energy per semi-cycle throughout the course of the rolling. The orange line is the linear fit of the points obtained from the previous analysis . So, its stable term (***p***) is connected to the linear damping coefficient $\boldsymbol{b_L}$ and its gradient (***q***) to the quadratic damping coefficient $\boldsymbol{b_q}$, all using the (4.23) expression.

BK10 – 20deg initial angle free roll test

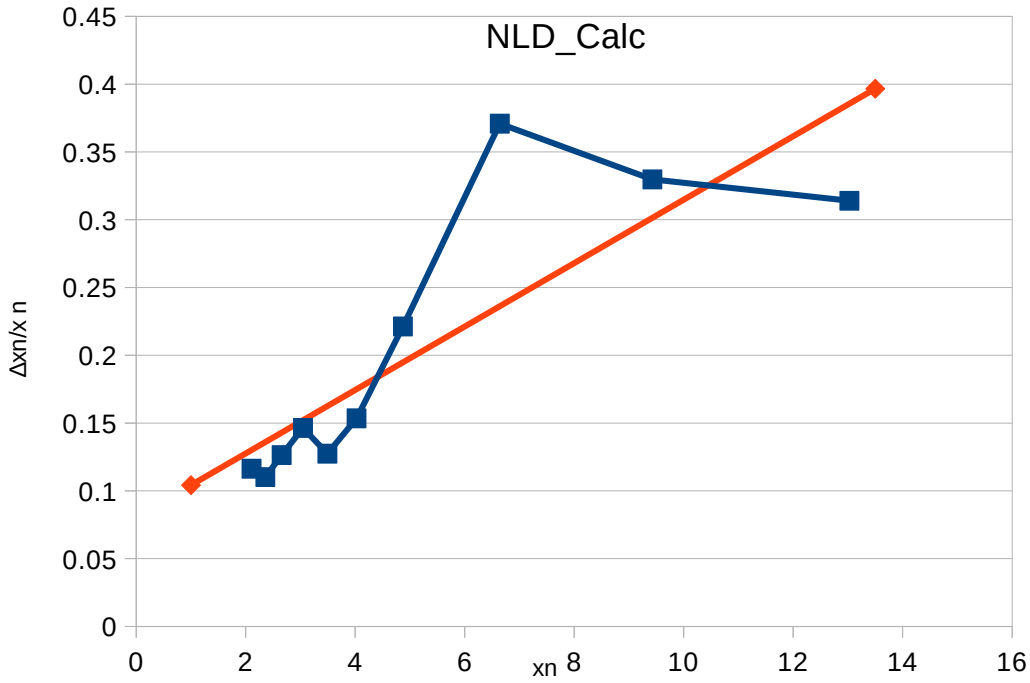

Figure 4.6.1 (a) : p – q analysis for the free rolling of BK10 at a 20 degree initial angle

By fitting the points linearly we can now calculate the linear and the quadratic part of the damping and so,

bl	***bq***
0.0532	0.0034

Regarding the modules, the $\boldsymbol{B_l}$ coefficient is measured in [N*m/(rad/s)] and $\boldsymbol{B_q}$ in [N*m/(rad/s^2)].

BK10 – 5deg initial angle free roll test

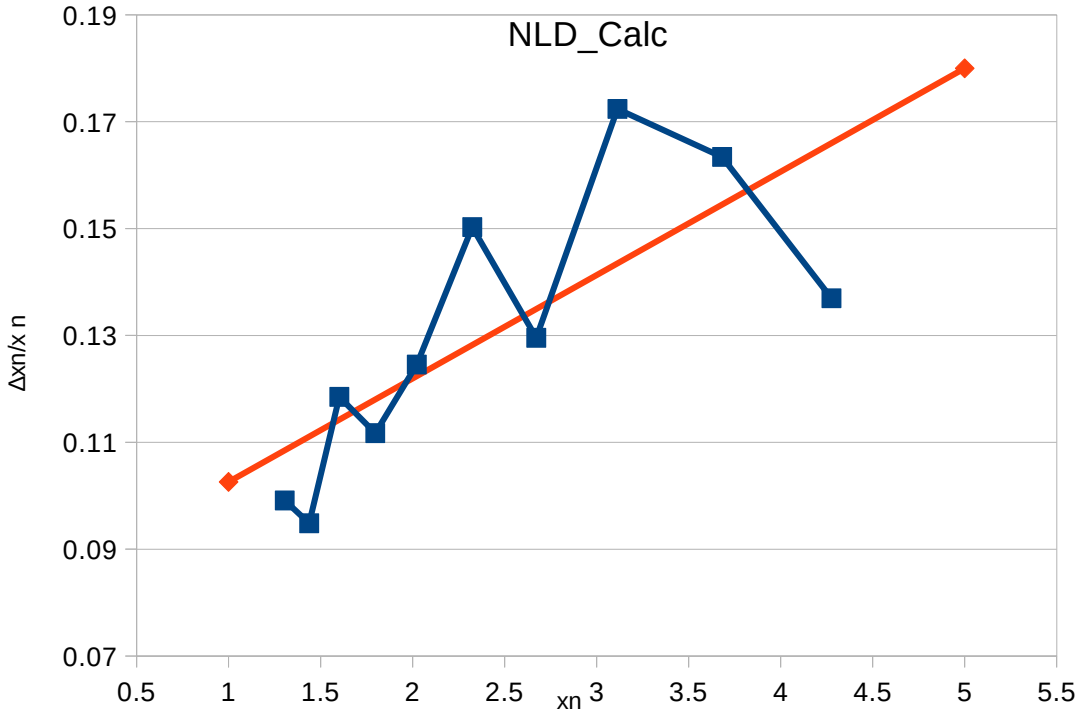

Figure 4.6.1 (b) : p – q analysis for the free rolling of BK10 at a 5 degree initial angle

bl	***bq***
0.0548	0.0028

As we expect the non-linear contributions in the damping increase as the initial angle increases.

4.4. FORCED ROLL TESTS

4.4.1.Wave Generation and Absorption

Considering a numerical wave tank, the generation of a desired wave profile along with the effective radiation of the outgoing waves out of the computational domain are two non insignificant problems. As Ntouras and Papadakis explain [8] the generation of a steadily progressive wave is performed by forcing the numerical solution, in a specific part of the computational space, to follow a wave solution provided by a wave theory. Moreover, an artificial damping of the waves is required and will be implemented near the solid boundaries of the wave tank. The boundary conditions, assume a uniform field and thus any physical disturbance created inside the domain should not reach the far-field boundary. Several types of methods can be applied to achieve that amount of absorption, such as coarsening the mesh as it approaches the solid boundaries. Although this technique is able to smear the solution, it does not guarantee zero reflection and so the boundaries are equipped with damping zones where the far-field conditions are applied.

In this work, the numerical generation and absorption of the free surface waves is performed through source terms applied in the momentum equations, in specific zones of the computational domain near the far-field boundaries. Usually, these zones extend for a few (2-3) wavelengths. The general form of the source terms is given by Equation (4.24). This source term drives the solution to the imposed $\boldsymbol{v}_{tar}$ velocity vector.

(4.24) $$\vec{S}_{nwt} = C_{nwt}\rho_m\left(\vec{v} - \vec{v}_{tar}\right)$$

The effect of the source terms is regulated through the $\boldsymbol{C}_{nwt}$ function and is described by equation (4.25)

(4.25) $$C_{nwt} = \alpha\frac{\exp\left(x_r^n\right) - 1}{\exp\left(1\right) - 1},\ x_r = \frac{x_s - x}{x_s - x_e}$$

$\boldsymbol{C}_{nwt}$ is a function of the non-dimensional position $\boldsymbol{x}_r$, where $\boldsymbol{x}_s$ and $\boldsymbol{x}_e$ the starting and ending point of the zone respectively. Typical values for the exponent $\boldsymbol{n}$ is between 2 and 5 and usually $\boldsymbol{\alpha}$ multiplier is not greater than 200.

4.4.2. Validation Approach

For the simulation of the wave excited forced roll test *MaPFlow* performed, we used a coarse grid (~130k cells) . The **Δs** value used for the boundary layer was 0.1 mm and the coarsening of the mesh, away from the hull, was regulated at a 1.2 aspect ratio. The free surface was set at a 0.6 m height from the bottom of the numerical tank, the generation zone of the wave was extended from position -11.0 m to position -7.8 m and the damping zone from position 8.0 m to 11.0 m . In contrast with the free decay tests, the grid was set thicker in the area between the generation zone and the barge. The reason behind that, was for the mesh to support the development and maintenance of the wave , to ensure the desired wave reaches the barge . In ***Fig.4.7.1(a)*** the experimental set up is provided along with the meshing of the numerical tank in ***Fig.4.7.1(b)*** .

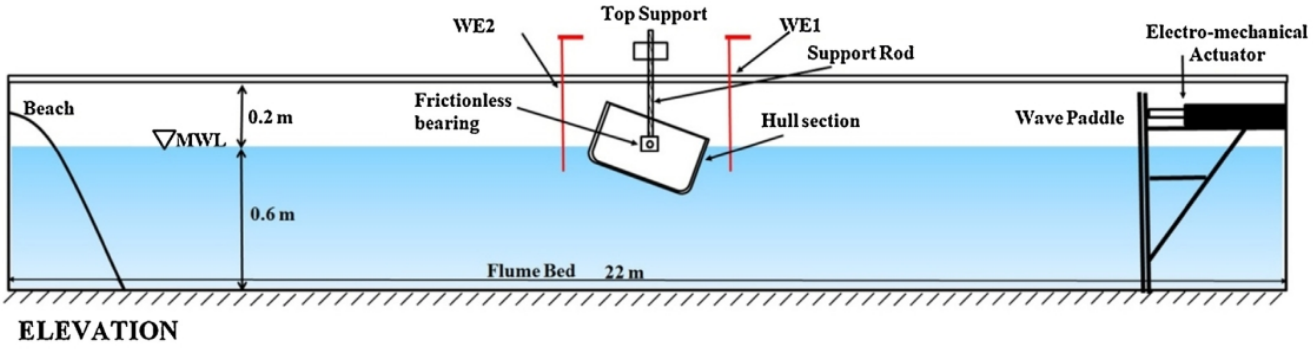

Figure 4.7.1 (a) : Experimental roll tank, IIT Madras.

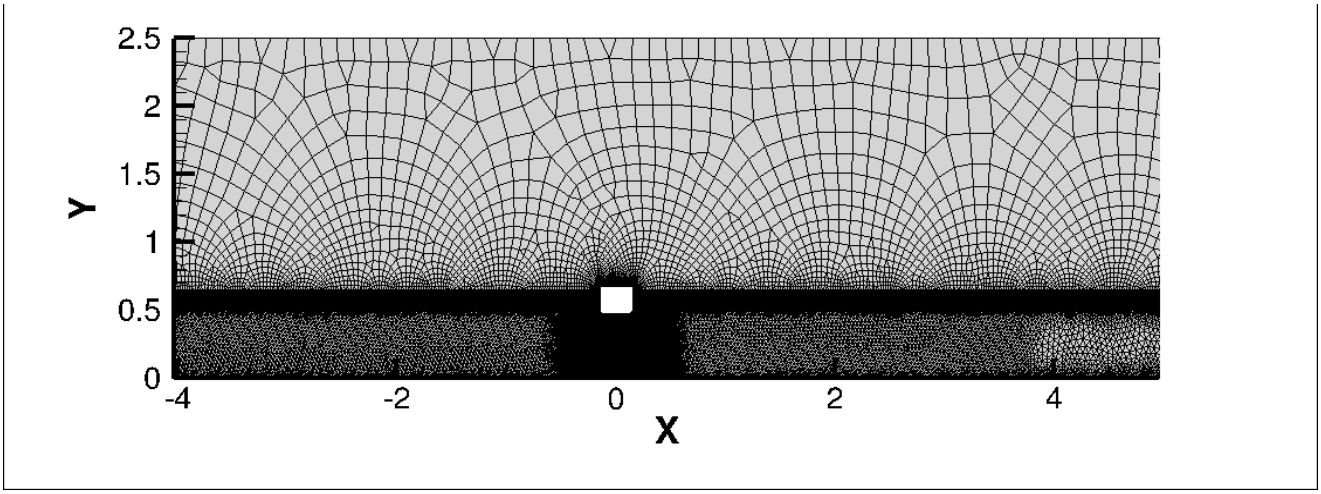

Figure 4.7.1 (b) : Meshing of the BK10 model for the forced roll simulations.

The obvious goal of the chapter is to check whether we can predict the roll response and damping of a hull section, under regular waves, using CFD solvers like *MaPFlow*. In order to validate the accuracy of our modeling we will compare the forced roll tests results performed by MaPFlow with experimental approaches made at Madras (India) Technological Institute by Irkal Mohsin A.R., S.Nallayarasu and S.K.Bhattacharyya in their work [14] “Experimental and CFD Simulation of Roll Motion of Ship with Bilge Keel” in 2014, using the same case set up. In the case which we will use for the validation we will excite the BK10 barge with regular waves of H=3 cm height near its natural period (T=1.2s) . In ***Figure 4.7.2*** it is noticeable that, according to the experiment we slightly underestimate the amplitude of the roll motion probably due to 3D effects. However, performing multiple forced roll tests for various excitation frequencies we can see that the deviation (in relation with the experimental data) remains constant.

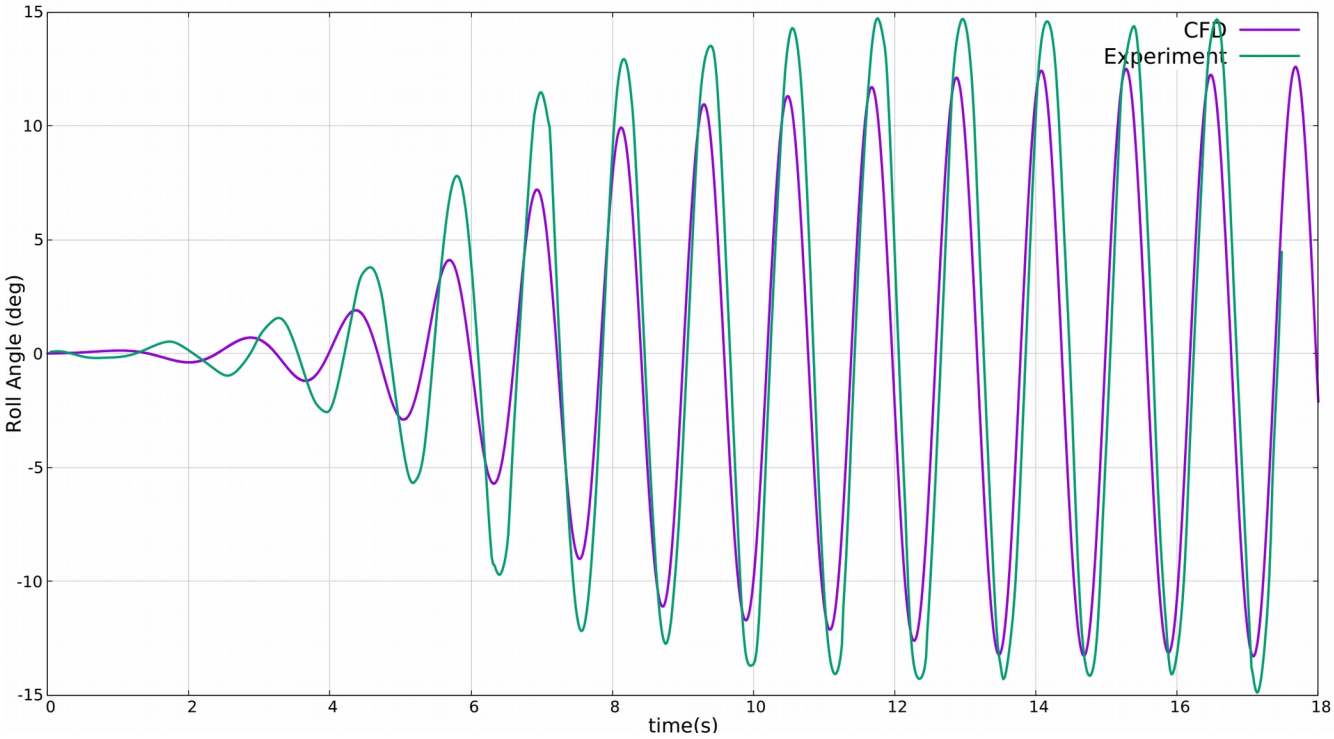

Figure 4.7.2: BK10 Roll Response under harmonic wave excitation

Having validated the accuracy of our solver to perform forced roll tests, we can now study the effect of the bilge keels in the roll response of a wave excited forced roll test.

4.4.3. Effect of the bilge keel on the Roll response

In order to have an outlook on the damping of the forced rolling system,two wave excited forced roll tests were done for BK00 and BK10. The wave input that was used for both tests is input E and is provided in ***Table 10.*** The results of the simulations were compared and their respective roll responses are shown in the following figures.

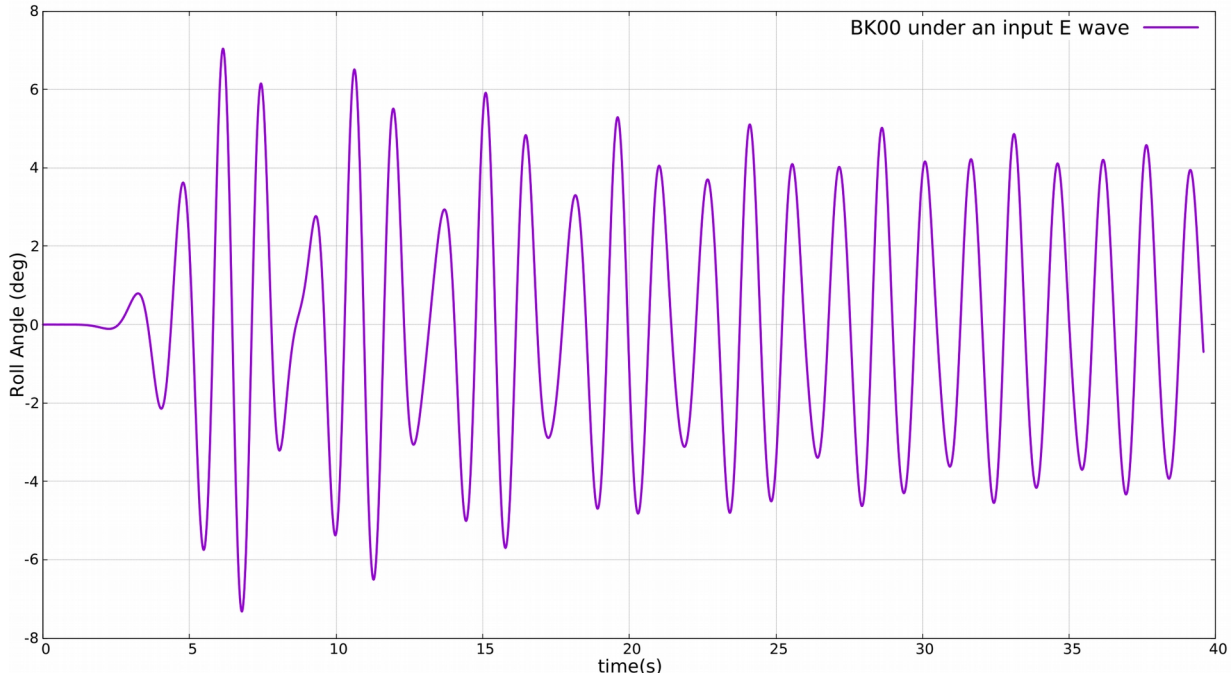

Figure 4.7.3 (a) : Roll Response of BK00 under a regular input E wave

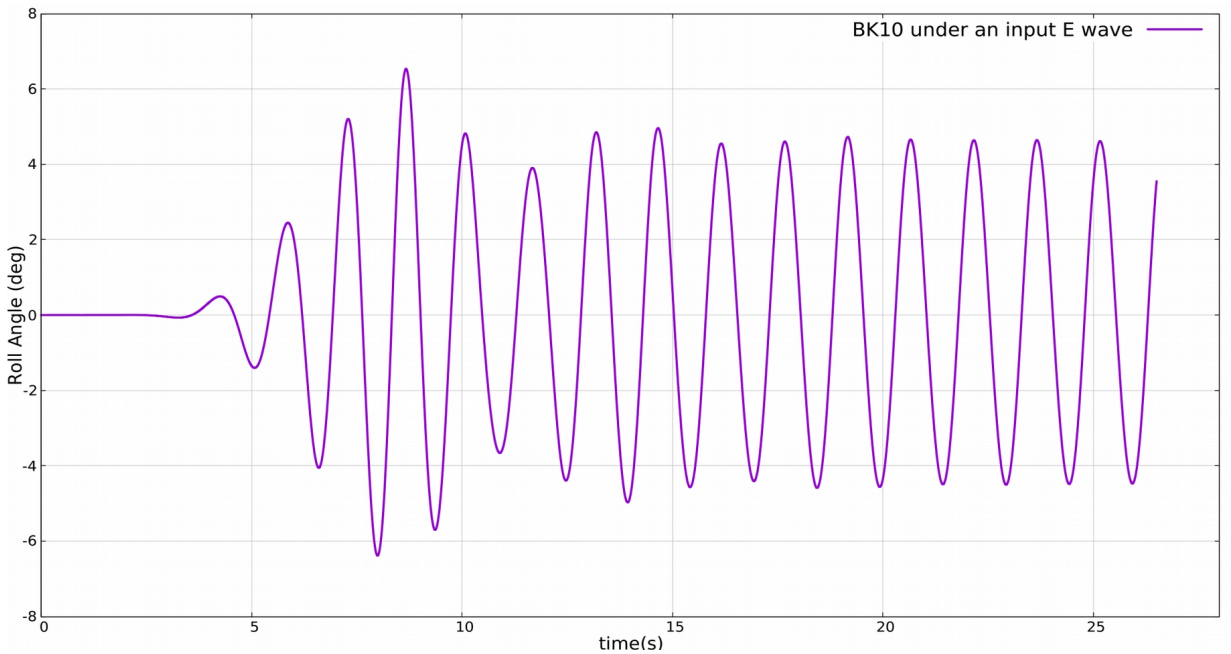

Figure 4.7.3 (b) : Roll Response of BK10 under a regular input E wave

Although the influence of the bilge keels seems to be small in the roll amplitude, that is expected looking back at previous simulations and experiments reproduced for the same barge and the same set up [14]. We expect the effect of the bilge keels to be more significant on the roll response, for wave inputs closer to the natural period however *MaPFLow* could not handle this amount of mesh deformation at this moment of time.

Reaching this point, it is now valuable to see how the bilge keels affected the vorticity field in the previously mentioned forced roll simulations, and so :

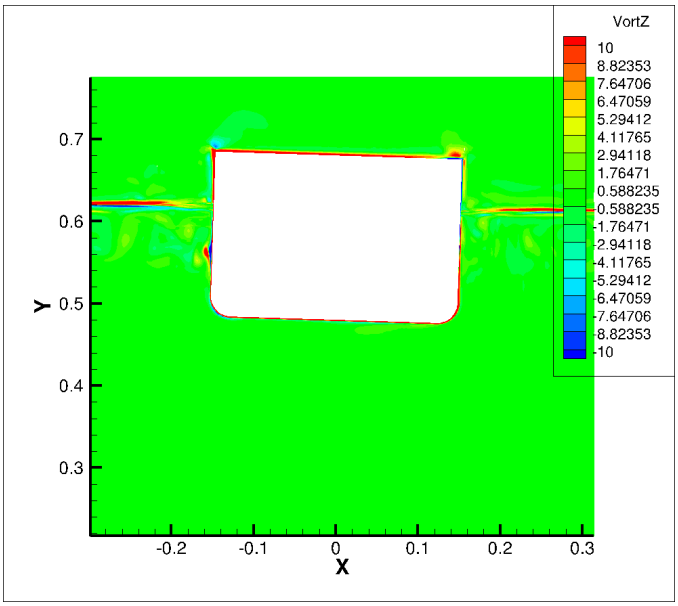

Figure 4.7.4 (a): Vorticity field around BK00

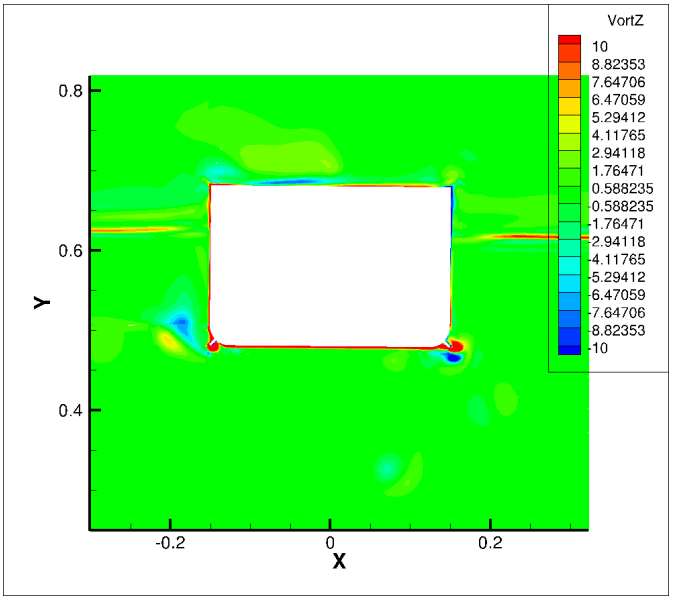

Figure 4.7.4 (b): Vorticity field around BK10

It needs to be mentioned that there is a non neglected difference between the refinements of the two meshes in the downside area of the barge. In the BK10 case a sizebox has been applied, allowing a maximum length surface of 5 mm^2 and a growth rate of 1.005 for the control surfaces (2D) as shown below.

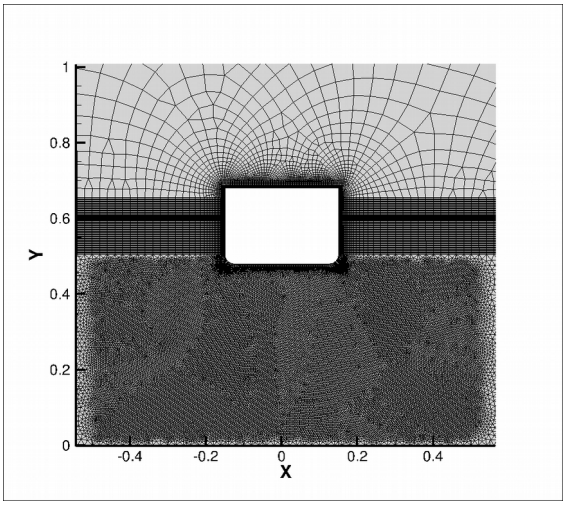

Figure 4.7.4 (c): BK10 mesh sizebox under the bilge keels

Along with the validation case, as said, four more simulations were performed and their wave input (A,B,D,E) is shown in ***Table 10.***

	A	B	C	D	E
Time Period	1.000 s	1.125 s	1.200 s	1.375 s	1.500 s
Height	3 cm	3 cm	3 cm	3 cm	3 cm

Table 10: "*Wave Inputs"*

Their respective roll amplitudes of motion are shown in ***Figure 4.4.5*** along with the amplitudes obtained from the experimental results [14]. And so,

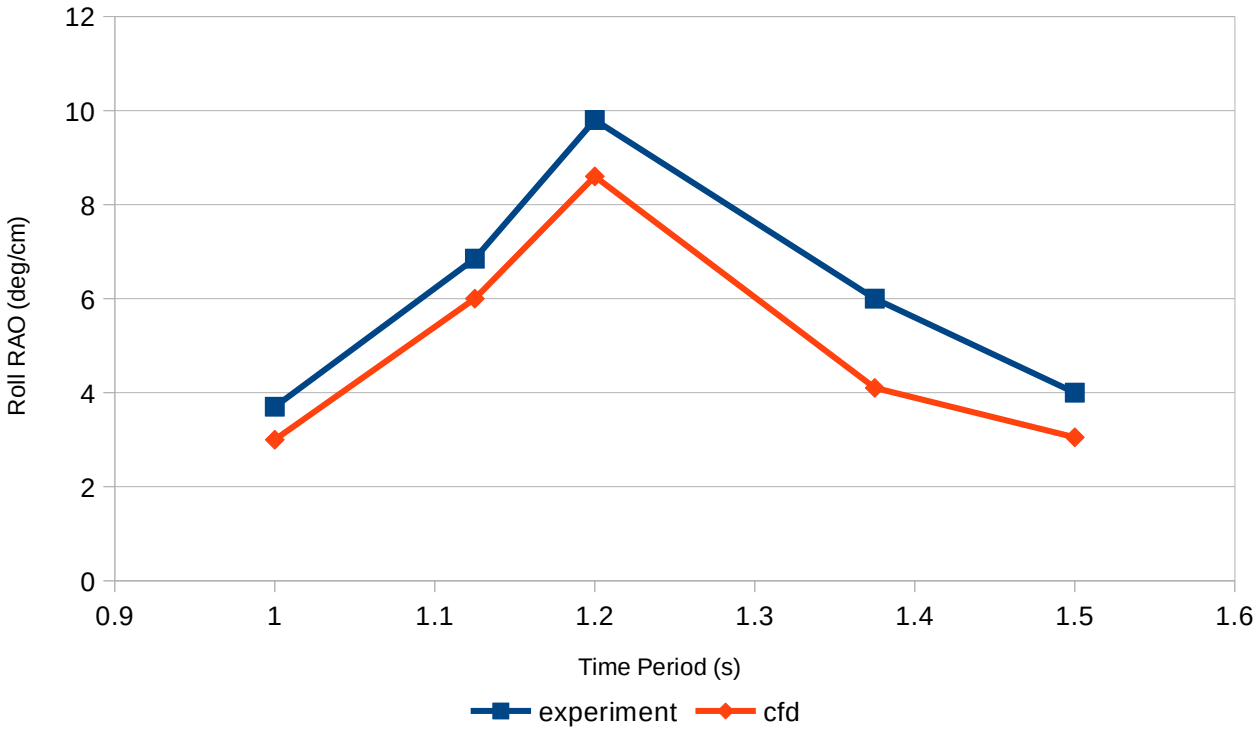

Figure 4.7.5: RAO comparison between CFD and experiment

4.5.Conclusions and Proposals for future work

The aim of this research was to investigate how the bilge keels affect the roll motion and especially the roll damping of a ship or a barge. For us to be able to implement this investigation, it was necessary to ensure that *MaPFLow* can perform free decay and forced roll simulations with sufficient accuracy.

For that reason free roll decay and forced roll tests were performed and then compared to experimental results obtained by previous studies [14], [16] . Looking at the results *MaPFlow* produced in total, we can see a sufficiently good agreement with the experiment, but a constant amount of deviation in the damping of the oscillations is also observed. It implies, that reproducing a 3D phenomena using a 2D model results in a loss of information which drives the response of the oscillations to constantly deviate from the experiment. This amount of information may refer to 3D flow phenomena or existence of friction between the barge and the rolling axis. It may be possible , to acquire the expected roll response and roll damping, or at least approach them, if multiple roll tests for various sections of the barge (or a ship) are performed and then integrated using strip theory [18].

As we observe the results, it has been clear that our 2D approximation of the 3D problem of roll motion leads in a not perfect agreement with the experimental results. The above mentioned loss of information sets the value of the 2D simulations to be limited. For that reason, a valuable proposal for future work is the performance of the 3D simulation . Another recommendation for a 3D simulation, is to perform a full scale simulation in an actual ship, for apparent reasons.

Furthermore, having our 2D model working sufficiently well (but not perfect), an investigation of the optimal bilge keel geometry could also be implemented. Regarding to the forced roll system, a damping analysis could also be developed in order to calculate the damping coefficients or the damping ratio (or the equivalent damping ratio in the non linear approximation).

Summarizing the results of our work, we now have a much clearer view of the influence of the bilge keels in roll motion. The impact of the bilge keels in roll damping is apparently positive occurring a significant decrease in the roll amplitude of the barge, causing also a small decrease in the ship’s natural period. The non-linear damping tends to increase as the initial angle increases, as expected. We also expect the non-linear effects to magnify as we add the bilge keels to the barge, although that type of analysis was not performed.

BIBLIOGRAPHY

[1] Y. Ikeda, Y. Himeno, N. Tanaka. Components of Roll Damping of ship at forward speed. University of Osaka Prefecture, School of Naval Engineering, August 1978.

[2] Y. Ikeda, Y. Himeno, N. Tanaka. On Eddy making component of Roll Damping Forced in Naked Hull. University of Osaka Prefecture, School of Naval Engineering, July 1978.

[3] Y. Himeno. Prediction of the ship Roll Damping – State of the art. The University of Michigan, College of Engineering, September 1981.

[4] Korpus, R. and Falzarano, J. (1997), "Prediction of viscous ship roll damping by unsteady Navier-Stokes techniques", *J. Offshore Mech. Arct. Eng.*,

[5] Arne Braathen and Odd M Faltinsen. Interaction between shed vorticity, free surface waves and forced roll motion of a two-dimensional floating body. *1988 IOP Publishing Ltd*.

[6] F. Jaouen, A. H. Koop, and G. Vaz. Predicting roll added mass and damping of a ship hull section using cfd. Proceedings of the International Conference on Offshore Mechanics and Arctic Engineering – OMAE, 7, 01 2011. doi: 10.1115/OMAE2011-49085.

[7] F. Jaouen, A. H. Koop, G. Vaz, and G. Crepier. RANS predictions of roll viscous damping of ship hull sections. V International Conference on Computational Methods in Marine Engineering, MARINE 2011, 2011.

[8] Γ.Α. ΑΘΑΝΑΣΟΥΛΗΣ, Κ.Α. ΜΠΕΛΙΜΠΑΣΑΚΗΣ, "ΔΥΝΑΜΙΚΗ ΠΛΟΙΟΥ". Πανεπιστημιακές εκδόσεις ΕΜΠ, Αθήνα 2012.

[9] Manolas, D. Hydro-aero-elastic Analysis of Offshore Wind Turbines. Ph.D. Thesis, National Technical University of Athens, School of Mechanical Engineering, Zografou, Greece, 2015.

[10] D.Ntouras, G.Papadakis . A Coupled Artificial Compressibility Method for Free Surface Flows. Journal of Marine Science and Engineering, August 2020.

[11] Queutey, P.; Visonneau, M. An interface capturing method for free-surface hydrodynamic flows. Comput. Fluids 2007, 36, 1481–1510, doi:10.1016/j.compfluid.2006.11.007.

[12] Menter, F.R. Two-equation eddy-viscosity turbulence models for engineering applications. AIAA J. 1994,
32, 1598–1605, doi:10.2514/3.12149.

[13] Y. Zhao, J. Tai, F. Ahmed. Simulation of micro flows with moving boundaries using high-order upwind FV method on unstructured grids. *Computational Mechanics* **volume 28**, 66–75 (2002).

[14] Irkal Moshin A.R., S.Nallayarasu, S.K.Bhattacharyya. Experimental and CFD simulation of Roll motion of ship with Bilge keel. MARHY 2014.

[15] Papadakis, G. Developement of a hybrid compressible vortex particle method and application to external problems including helicopter flows. NTUA, December 2014.

[16] Irkal Moshin A.R., S.Nallayarasu, S.K.Bhattacharyya. CFD approach to roll damping of ship with bilge keel with experimental validation. Applied Ocean Research Volume 55, February 2016, Pages 1-17.

[17] Δυναμική Ευστάθεια Πλοίου, Κ. ΣΠΥΡΟΥ, Κάλλιπος 2014.

[18] S. A. W. Smaal , “Roll Damping Prediction Method: To determine linear and non-linear roll damping coefficients based on multiple 2D CFD simulations”, MSc thesis , Dpt. Of Marine Technology, T.U.Delft, August 2019.